Younger Dryas and Early Holocene Climate in South Greenland Inferred from Oxygen Isotopes of Chironomids, Aquatic Moss, and Moss Cellulose

Peter J.K. Puleo[1], Andrew L. Masterson[1], Andrew S. Medeiros[2], Grace Schellinger[1], Regan Steigleder[1], Sarah Woodroffe[3], Magdalena R. Osburn[1], Yarrow Axford[1]

1. Department of Earth and Planetary Sciences, Northwestern University, Evanston, IL, 60201
2. School for Resource and Environmental Studies, Dalhousie University, Halifax, Nova Scotia, Canada, B3H 4R2
3. Department of Geography, Durham University, Lower Mountjoy, South Road, Durham, UK, DH1 3LE

Corresponding Author: Peter Puleo; peterpuleo2024@u.northwestern.edu
2145 Sheridan Road, Room F480
Evanston, IL, 60201

Keywords: Younger Dryas, Holocene, Greenland, Paleoclimatology, Paleolimnology, Deglaciation, Stable Isotopes, Micropaleontology, Diatoms, Chironomids

Abstract

Ice core records have long indicated that the Younger Dryas began and ended with large, abrupt climate shifts over Greenland. Key climatic features remain unknown, including the magnitude of warming during the Younger Dryas-Holocene transition along with the seasonality and spatial variability of Younger Dryas climate changes across Greenland. Here, we use geochemical and paleoecological proxies from lake sediments at Lake N14 in south Greenland to address these outstanding questions. Radiocarbon dating and diatom assemblages confirm early deglaciation and isolation of Lake N14 before ~13,600 cal yr BP, consistent with previous work. Oxygen isotope ratios ($\delta^{18}O$) of chironomid head capsules, bulk aquatic moss, and aquatic moss-derived cellulose are used to reconstruct oxygen isotopes of past lake water and annual precipitation. Oxygen isotope proxies indicate annual precipitation $\delta^{18}O$ values increased by 5.9 - 7.7‰ at the end of the Younger Dryas. Following the Younger Dryas, moss and cellulose $\delta^{18}O$ values show a clear decline in precipitation $\delta^{18}O$ values of 2 - 3‰ from ~11,540 - 11,340 cal yr BP that may correspond with the Preboreal Oscillation. Reconstructed precipitation $\delta^{18}O$ values then gradually increased from 11,300 - 10,100 cal yr BP. All three aquatic organic materials register similar shifts in precipitation $\delta^{18}O$ values over time, and they closely parallel the $\delta^{18}O$ shifts observed in ice cores. This evidence strongly supports the utility of these methods for reconstructing lake water $\delta^{18}O$, and furthermore precipitation $\delta^{18}O$ values where lake water reflects precipitation. The relatively large shift in isotopic composition of precipitation at Lake N14 suggests that shifts in temperature, precipitation seasonality, and/or moisture sources at the end of the Younger Dryas were even larger in south Greenland than they were in central Greenland, most likely because of the proximity to major changes in North Atlantic Ocean circulation. The annual air temperature change estimated at Lake N14 at the end of the Younger

Dryas is also very large (~18 ± 7°C) compared to the summer warming previously inferred from chironomid species assemblages there (~6°C). This indicates that the strongest warming at the end of the Younger Dryas occurred in the winter season, consistent with past observations of intensified Younger Dryas seasonality at Lake N14 and elsewhere in Greenland.

1. Introduction

Large and rapid temperature and ice sheet fluctuations occurred in Northern Hemisphere high latitudes from the Last Glacial Maximum to the early Holocene (Alley and Clark, 1999; Shakun and Carlson, 2010). One key event was the Younger Dryas cold event (YD; ~12,900 - 11,700 cal yr BP [calibrated years before present, where present is 1950 CE]), characterized by cold and dry conditions around the North Atlantic and beyond. The transition from the YD to the early Holocene resulted in a temperature increase of ~15 ± 3°C in central Greenland over ~1500 years, with 5 - 10°C of this warming occurring in a few decades or less (Severinghaus et al., 1998; Alley, 2000). Much of this warming is thought to have occurred in the winter season, indicating the Younger Dryas featured heightened seasonality (summer-winter air temperature difference; Denton et al., 2005). Additionally, Greenland ice core records (DYE3 and GISP2) suggest an inverse relationship between YD temperature change and latitude in Greenland, with the southern parts of Greenland experiencing the largest temperature shifts (Buizert et al., 2014; Buizert et al., 2018).

The cause of the YD was likely related to Laurentide Ice Sheet decay following the Last Glacial Maximum, which is relevant for understanding the context of future climate changes as the Greenland Ice Sheet retreats due to anthropogenic warming. Near the YD onset, an outburst

of meltwater likely flowed into the North Atlantic (Broecker et al., 1988; Alley, 2000; Carlson et al., 2007; Leydet et al., 2018; cf. Keigwin et al., 2018) and slowed Atlantic Meridional Overturning Circulation (AMOC) by inhibiting deep water formation (McManus et al., 2004). Other hypotheses suggest atmospheric circulation changes (Renssen et al., 2015) or an extraterrestrial impact (Firestone et al., 2007) may have also been involved. A North Atlantic origin of the YD could explain why the magnitude of cooling appears to decrease with increasing latitude in Greenland (Buizert et al., 2014; Buizert et al., 2018), as the AMOC transports significant heat to the area around southern Greenland. The AMOC forcing is also consistent with hypothesized seasonality changes in the YD (Denton et al., 2005). Today, significant volumes of meltwater from glaciers and ice sheets may be weakening AMOC and causing colder surface water temperatures just off the coast of south Greenland (Rahmstorf et al., 2015; Caesar et al., 2021). In any case, AMOC is expected to weaken in the future in response to anthropogenic warming (Jackson et al., 2022), making the YD relevant to future climate change.

Following the YD, the early Holocene (~11,700-8200 cal yr BP) saw continued elevated Northern Hemisphere summer insolation and further regional deglaciation (Briner et al. 2016; Axford et al., 2021). The early to middle Holocene is the most recent and well-studied period of warming with summer temperatures in many parts of Greenland higher than those of the 20th Century, and hints of the largest temperature anomalies occurring at the highest latitudes in northern Greenland (Axford et al., 2021). The onset of Holocene warmth may have varied regionally, with some glacial evidence suggesting parts of south and southwest Greenland warmed above 20th Century summer temperatures several thousand years later than other parts of Greenland (Larocca et al., 2020; Axford et al., 2021). The Preboreal Oscillation (~11,500 - 11,300 cal yr BP; Rasmussen et al., 2007) falls within the early Holocene. It was a relatively

abrupt cooling period of smaller magnitude (~2‰ decrease in Greenland ice core $\delta^{18}O$ values; Rasmussen et al., 2007) and duration (~100-200 years; Rasmussen et al., 2007) than the YD. Evidence for this event comes from a wide range of archives in Greenland and Europe, including tree rings, lake sediment cores, glacial moraines, and ice cores (Björck et al., 1997; Fiłoc et al., 2018). The origin of the event is also thought to be from meltwater inputs leading to an alteration of AMOC strength (Björck et al., 1997), much like the YD.

South Greenland is a key location for developing new paleoclimatic records over the deglacial period due to its proximity to the North Atlantic Deep Water formation zone, which plays a role in AMOC, and to the Greenland Ice Sheet, which influences sea level and is the source of multiple ice core records (Grootes and Stuiver, 1997; Dansgaard et al., 1982; Badgeley et al., 2020). Records from south Greenland, especially quantitative temperature reconstructions, are sparse (Badgeley et al., 2020). Here, we target Lake N14, an isolation basin that was previously shown to contain sediments spanning the last ~13,800 years (Bennike and Björck, 2000; Björck et al., 2002). This is the only known location in Greenland that contains a sediment record of the entire YD.

In this study we develop a series of paleoclimatological and paleoenvironmental proxies from Lake N14. We do this to elucidate regional climatic variability, examine the extent of YD seasonality and to supplement ice core-based records of climatic change in Greenland from the Bølling-Allerød (BA) to the early Holocene. The proxies include bulk sediment geochemistry, magnetic susceptibility, diatom assemblages, chironomid assemblages, and the oxygen isotope ratios ($\delta^{18}O$) of chironomid head capsules, bulk aquatic moss macrofossils, and aquatic moss-derived cellulose. We use sediment chemistry, magnetic susceptibility, and diatom assemblages to assess the timing of the onset of lacustrine sedimentation, i.e., isostatic emergence of the lake

during deglaciation (Long et al., 2011), and to constrain when the site deglaciated (Björck et al., 2002; Levy et al., 2020). Chironomid assemblages were used in a previous study at Lake N14 to infer summer air temperatures (Medeiros et al., 2022), which drive ice sheet and glacial melt. Finally, the $\delta^{18}O$ values of aquatic organic materials reflect lake water $\delta^{18}O$ values ($\delta^{18}O_{lw}$), which are largely derived from annual precipitation $\delta^{18}O$ values in the study setting (Wooller et al., 2004; Zhu et al., 2014; Lasher et al., 2017; van Hardenbroek et al., 2018). These $\delta^{18}O$ values can be compared to nearby ice core records and used to estimate changes in precipitation $\delta^{18}O$ values, and by extension, to constrain temperature change. In combination, these proxies can help answer lingering questions about regional climate variability and seasonality changes from ~13,600 to 10,100 cal yr BP.

2. Site Description

Lake N14 (59°58.85'N, 45°10.80'W; 33 m a.s.l.; Fig. 1B) is located on Angissoq Island, ~9 km off the coast of south Greenland. N14 is an isolation basin, suppressed below local sea level until isostatic rebound lifted it from the sea (Björck et al., 2002). Lake N14 is approximately 130 m long by 130 m wide with a maximum water depth of ~8.5 m. It is precipitation fed and through flowing, with a single outflow to the west that is active in late summer. The estimated modern open-water season (season with at least an ice-free moat) at Lake N14 is ~May-October based on climate data from Qaqortoq (Cappelen, 2019) and observations from satellite imagery. The bedrock around Lake N14 is Paleoproterozoic aged granite and granodioritic gneiss (Steenfelt et al., 2016), and the vegetation is dwarf-shrub tundra (Andresen et al., 2004).

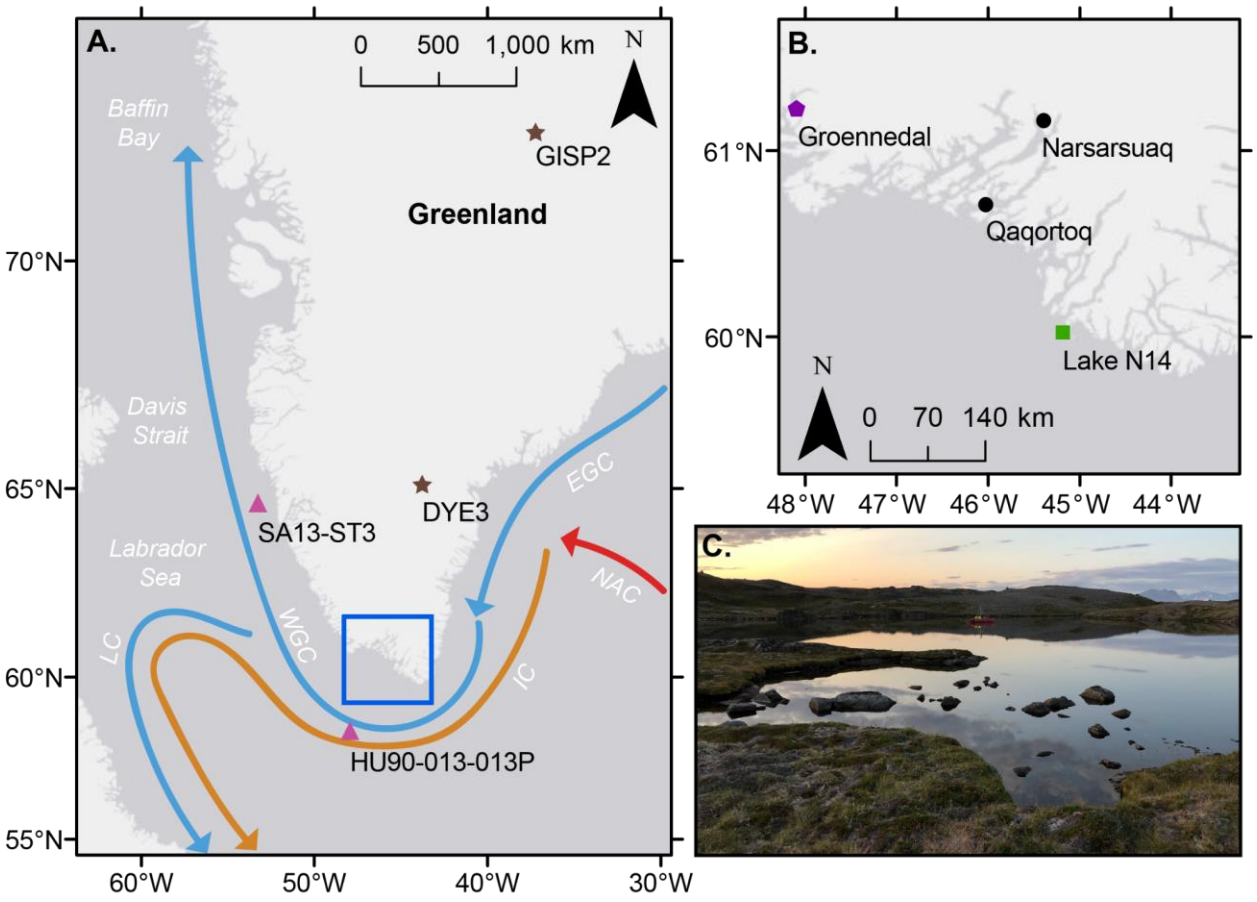

Fig. 1 (A) An overview of Greenland with key ocean currents (NAC=North Atlantic Current, EGC=East Greenland Current, IC=Irminger Current, WGC=West Greenland Current, LC=Labrador Current). Brown stars indicate locations of the GISP2 (72°58.2'N, 38°48.0'W) and DYE3 (65°10.8'N, 43°49.2'W) ice core sites. Pink triangles indicate the locations of marine sediment cores HU90-013-013P (58°12.59'N, 48°22.40'W) and SA13-ST3 (64°26.74'N, 52°47.64'W). Blue box indicates the extent of panel B. (B) The setting of Lake N14 (green square) in southernmost Greenland. Also shown are the towns of Qaqortoq and Narsarsuaq (black dots) and the Groennedal Global Networks of Isotopes in Precipitation (GNIP) station (purple pentagon). (C) Lake N14 in August 2019. Photo taken by Peter Puleo.

Modern (1981-2010 CE) precipitation amounts range from 6.3 cm in March to 10.7 cm in August with a total of 96.3 cm annually (Fig. 2A) at a coastal weather station near Lake N14 (Qaqortoq, ~85 km north-northwest; Fig. 1B). Precipitation is slightly higher in the late summer and early fall, with approximately half of the precipitation falling between July-November (Cappelen, 2019). Modern temperatures range from -5.9°C in February to 7.7°C in August (Cappelen, 2019; Fig. 2B). The Global Network of Isotopes in Precipitation station of Groennedal in south Greenland (~210 km northwest of the site; Fig. 1B) recorded monthly oxygen and hydrogen isotopes of precipitation from 1961-1974 CE (IAEA/WMO, 2015; Fig. 2C), allowing for the formation of a local meteoric water line near Lake N14 (LMWL; $\delta^2H = 6.4*\delta^{18}O - 15.4$; $r^2 = 0.89$; n = 70; Fig. 2D). The measurements of N14 lake water (collected late July and early August 2019; n = 3) fall directly on this LMWL (average $\delta^{18}O = -8.3 \pm 0.3‰$, average $\delta^2H = -67.4 \pm 1.0‰$), indicating Lake N14 is not highly influenced by evaporation (Fig. 2D). The single precipitation (rainfall) event sampled from Lake N14 in the field (August 3rd, 2019) falls outside the range of values measured at Groennedal and just below the LMWL ($\delta^{18}O = -2.9 \pm 0.06‰$, $\delta^2H = -42.0 \pm 0.2‰$; Fig. 2D). Water from other south Greenland lakes near Narsaq was collected in August 2016 (Lasher and Axford, 2019; Fig. 2D).

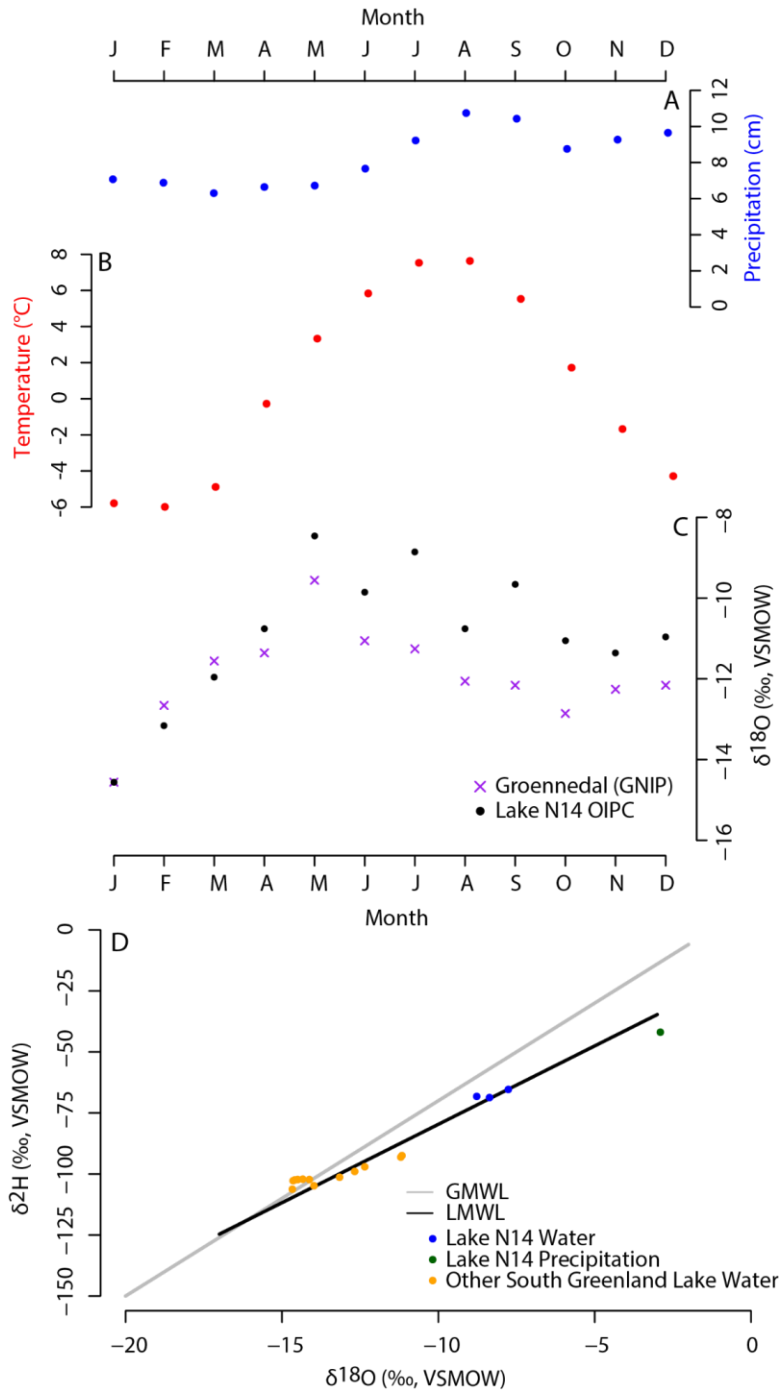

157

158 **Fig. 2** Monthly precipitation amount (A) and temperature (B) from the Qaqortoq weather station
159 (Cappelen, 2019) alongside monthly precipitation isotope measurements (C) from the
160 Groennedal station (IAEA/WMO, 2015) and modeled monthly precipitation isotopes from the
161 Online Isotopes in Precipitation Calculator (Bowen, 2022; Bowen et al., 2005; IAEA/WMO,

2015). (D) The global meteoric water line (GMWL) and local meteoric water line (LMWL; based on data from the Groennedal GNIP station (IAEA/WMO, 2015)) are plotted alongside measured values of Lake N14 lake water and precipitation, and measured values from other south Greenland lakes sampled in the Summer of 2016 (Lasher and Axford, 2019).

3. Methods

3.1 Core Collection and Processing

In August 2019, we collected a ~380 cm long sediment core (19-N14-N7) using a Nesje percussion piston corer from near the middle of Lake N14 at 4.2 m water depth. Here we focus on the lowermost section of this core (19-N14-N7 bot), which contains late glacial and early Holocene sediments. Cores were split using a GeoTek core splitter at Northwestern University and stored at 4°C. Sediment elemental concentrations (Ti, S), color, and magnetic susceptibility (MS) were analyzed at 0.5 cm resolution on split core sections using a GeoTek Multi-Sensor Core Logger (MSCL-S) equipped with an Olympus Delta X-ray fluorescence (XRF) analyzer, a Bartington MS2E magnetic susceptibility meter, and a 50 mm Canon camera. The XRF estimates abundances of some elements and is most reliably used for assessing relative changes in elemental concentration (Boyle, 2000). The uncertainty of the elemental concentrations is ~5 - 10% and varies by element. Magnetic susceptibility assesses relative changes in the magnetic minerogenic content of the sediment (Francus et al., 2009). The camera provides a high-resolution image of the 19-N14-N7 core.

3.2 Age-Depth Model

Geochronology is based upon Accelerator Mass Spectrometry (AMS) radiocarbon ages obtained on aquatic mosses (n = 18) as well as 1-cm-thick bulk sediment samples in zones where plant macrofossils were limited or absent (n = 6; Table 1). Twenty-three of the 24 samples were processed and analyzed at the Woods Hole Oceanographic Institution National Ocean Sciences Accelerator Mass Spectrometry (WHOI NOSAMS) facility, while one sample was analyzed by Beta Analytic. The age model was created using the R package Bacon v2.5.5, which uses a Bayesian statistical approach for age-depth modeling (Blaauw and Christen, 2011). Radiocarbon ages were calibrated using Calib version 8.2 (Stuiver et al., 2022) and the IntCal20 calibration curve (Reimer et al., 2020).

3.3 Chironomid and Diatom Species Assemblages

Diatoms were analyzed at 1 cm intervals through the top 4 cm of the basal gray minerogenic unit and into the overlying laminated, organic-rich gyttja, continuing through the gray unlaminated silt-rich layer and into the laminated moss-rich gyttja above. Diatom samples were taken using standard methods (Palmer and Abbott, 1986) with diatom identifications made with reference to Van der Werff and Huls (1958-74), Hustedt (1957), Patrick and Reimer (1966, 1975), Hendey (1964) and Foged (1972, 1973, 1977). The diatom nomenclature was updated to the most recent taxonomic concepts using the Diatoms of North America online database (Spaulding et al., 2021). A minimum of 250 valves were counted at each interval. A combination of diatom data and the lithostratigraphy of the core was used to identify isolation contacts, following procedures outlined in Long et al. (2011).

Chironomid-based summer temperature reconstructions for the 19-N14-N7 core were previously reported in Medeiros et al. (2022), and detailed chironomid methods are given in that publication. We note that for five (of the eighteen total) samples reported, count sums from two to three adjacent samples were combined to reach total sums >50 whole head capsules; these samples' depths are reported as the mid-depth of the overall range of depths represented by the combined sample. In addition, three samples had final count sums <50 head capsules despite combining adjacent samples; all three samples with low final count sums are from a moss-dominated section of the core with very low chironomid concentrations (<1 head capsule g^{-1}). Summer air temperatures (mean temperatures of the warmest quarter, approximately equivalent to June-July-August) were reconstructed using a 2-component weighted averaging partial-least-squares (WA-PLS) model with a RMSEP of 1.59 °C. Based on chironomids in a surface sediment sample from Lake N14 (0-2 cm depth), the model of Medeiros et al. (2022) estimated a summer temperature of 7.0 °C, which is statistically indistinguishable from the meteorological JJA temperature (for 1981-2010 CE) of 7.1 °C at Qaqortoq. Here we use that estimate of 7.0 °C as the baseline for expressing temperature reconstructions as anomalies versus modern.

3.4 $\delta^{18}O$ of Aquatic Organic Materials as a Proxy for Lake Water and Precipitation $\delta^{18}O$

Chironomid head capsule $\delta^{18}O$ values primarily reflect lake water $\delta^{18}O$ ($\delta^{18}O_{lw}$) values (calibrated to VSMOW) as the aquatic larvae develop (Wooller et al., 2004). Recently, Corcoran et al. (2021) have suggested chironomid head capsules reflect late summer $\delta^{18}O_{lw}$ values and, therefore, summer-biased mean annual precipitation (where groundwater and evaporative effects are minimal). This conclusion stems from evidence that some species of Arctic chironomids

transition from third to fourth instar (larval stage) in the late summer or early fall (Butler and Braegelman, 2018). However, we note that various Arctic taxa likely have different timings for the third to fourth instar transition (Tokeshi, 1995; Butler and Braegelman, 2018), can grow throughout the year (Oliver, 1968; Butler, 1982; Tokeshi, 1995), and can take multiple years to complete their larval life cycles (Oliver, 1968; Butler, 1982; Tokeshi, 1995; Butler and Braegelman, 2018). Therefore, we interpret our chironomid $\delta^{18}O$ values to reflect $\delta^{18}O_{lw}$ values throughout the entire summer and probably longer durations. Aquatic mosses also reflect $\delta^{18}O_{lw}$ values as they grow (Zhu et al., 2014) and they require light for growth. Because of this, they likely record $\delta^{18}O_{lw}$ values over the ice-free season and to a lesser extent the spring and fall when some sunlight may penetrate through lake ice (Riis et al., 2010). This roughly overlaps with the likely timing of maximum chironomid larvae growth.

Hydrologic controls ultimately determine the $\delta^{18}O_{lw}$ values of lake water used by organisms for biosynthesis at any given time. Average modern lake water residence time at Lake N14 is estimated to be ~0.9 years. We roughly estimate average residence time by dividing a lake volume estimate (~67,500 m^3) by the Qaqortoq annual precipitation amount (0.96 m; Cappellan, 2019) times the lake's watershed area (77,950 m^2; calculated using the ESRI ARCMap Hydrology toolset and a 2 m resolution DEM (ArcticDEM; Porter et al., 2018). A residence time of just under 1 year suggests that an organism growing only in summer would incorporate waters partly derived from cold-season precipitation. We argue that in summer Lake N14 contains a mix of snowmelt carrying cold-season precipitation and summer rainfall, with decreasing influence of winter and spring precipitation as the growing season progresses. Therefore, chironomid and aquatic moss $\delta^{18}O_{lw}$ values, which reflect lake water throughout summer at a minimum, reflect annually integrated precipitation isotopes.

Controls on lake water and precipitation isotopes at Lake N14 were undoubtedly different during the YD. Strongly reduced YD precipitation (Alley, 2000) would increase average lake water residence time and thus possibly increase evaporative influence on lake water isotopes. Longer duration of ice cover, on the other hand, would suppress evaporation. If winter precipitation was reduced more dramatically than summer as has been posited for the YD (Alley, 2000), then lake water would reflect a more summer-biased mean annual precipitation $\delta^{18}O$ value, potentially reducing the magnitude of $\delta^{18}O_{lw}$ changes into and out of the YD (as winter precipitation has more negative $\delta^{18}O$ values than summer precipitation). Regional climate shifts associated with the YD also included changes in sea-surface temperatures and sea ice cover, which in turn affected precipitation moisture source and path and thus isotopes of precipitation over Greenland (Nusbaumer et al., 2019).

3.5 Organic Material $\delta^{18}O$ Isotope Analyses and Interpretative Approach

To collect chironomid subfossil head capsules for $\delta^{18}O$ measurement, 5 - 15 cm^3 of sediment was sampled at a 1 - 5 cm resolution from 343.5 - 255.5 cm core depth. The sediment volume and resolution are variable given different abundances of chironomids in each sample. Samples were cleaned following modified methods from Verbruggen et al. (2010) and Clarke et al. (2019). We stirred samples in a beaker with 200 mL of a 10% KOH solution for 30 minutes, then wet sieved at 106 µm and rinsed them with DI water for ~5 minutes. The >106 µm fraction was stored in a centrifuge tube with DI water and placed in a cold room at 4°C. Chironomid head capsules were picked from these samples by hand under a dissecting microscope at 40X magnification. ~300 head capsules (~75 - 100 µg) from each sample were placed into a clean and

pre-weighed silver capsule. The samples were then freeze dried for five days to complete dryness and then analyzed for $\delta^{18}O$ values on a Thermo TC/EA, held at 1420°C, coupled with Delta V + IRMS via a Conflo IV interface. The TC/EA was equipped with a 1.5 m long molecular sieve 5A GC column to provide for separation and prevent co-elution of N_2 and analyte CO. Isotope standards used for analysis consisted of BaSO4 standards (NBS127, IAEA-SO5, and IAEA-SO6) and USGS water standards GISP, VSMOW, and UC03, along with an in-house chitin standard. Long term analytical precision of $\delta^{18}O$ values is ±0.4‰. Duplicates were completed for ~20% of the samples and averaged. Two of the three duplicates fell within 0.6‰ on average, which is slightly above the analytical uncertainty of 0.4‰. One set of duplicate samples (~10,800 cal yr BP) had the highest and lowest values of the record. These were omitted as we could not explain their disparate or extreme values.

Chironomid head capsule $\delta^{18}O$ values ($\delta^{18}O_{chi}$) were used to infer lake water $\delta^{18}O$ values ($\delta^{18}O_{lwchi}$) using Equation 1, which was generated by compiling modern $\delta^{18}O_{lw}$ and $\delta^{18}O_{chi}$ values (van Hardenbroek et al., 2018).

(1) $\delta^{18}O_{lwchi} = (\delta^{18}O_{chi} - 22.5) / 0.89$ (n = 50; $r^2 = 0.85$; RMSD = 2.3)

The data presented in this calibration are extensive and include sites from Europe, South America, Greenland, and Australia (van Hardenbroek et al., 2018). Modern lake water $\delta^{18}O$ values in the calibration range from -19 to 13‰. Because of the consistency of the $\delta^{18}O_{lwchi}$ - $\delta^{18}O_{chi}$ offset between the sites that span a large temperature range, it seems unlikely that lake water temperature has a large influence on isotope fractionation (Lasher et al., 2017), although recent evidence suggests a small temperature effect may exist (Lombino et al., 2021). The calibration data also represent a wide range of chironomid species and suggest there are not large

differences between species in fractionation effects, but species-specific vital effects have not been fully explored (Lasher et al., 2017). The combined analytical uncertainty and lake water regression uncertainty for $\delta^{18}O_{lwchi}$ is ±2.3‰.

To sample subfossil aquatic moss, identified as *Warnstorfia exannulata*, we collected 2-4 cm^3 of sediment every 1-2 cm from 327.0-261.5 cm. Mosses were not present below this depth. Samples were gently rinsed on a 250 µm sieve and the >250 µm fraction (which under a dissecting scope was observed to comprise entirely aquatic moss) was transferred to Whirl-Pak® bags and freeze dried for one day. Around 1 mg of this freeze-dried material from each depth was reserved for bulk moss $\delta^{18}O$ measurement, while the rest was used for cellulose extraction following Brendel et al. (2000). Samples of bulk moss and cellulose were then ground with a mortar and pestle, weighed into silver capsules, and freeze dried for five days. Bulk aquatic moss $\delta^{18}O$ ($\delta^{18}O_{moss}$) and aquatic moss cellulose $\delta^{18}O$ ($\delta^{18}O_{cell}$) were then measured in the same way as the chironomid head capsules with ~20% of samples duplicated.

$\delta^{18}O_{moss}$ was then used to infer lake water $\delta^{18}O$ values ($\delta^{18}O_{lwmoss}$) with Equation 2 (Zhu et al., 2014):

(2) $\delta^{18}O_{lwmoss} = 1.156*\delta^{18}O_{moss} - 32.2$ (n = 7; $r^2 = 0.995$; RMSD = 0.3)

$\delta^{18}O_{cell}$ was also used to infer lake water $\delta^{18}O$ values ($\delta^{18}O_{lwcell}$) with Equation 3 (Zhu et al., 2014):

(3) $\delta^{18}O_{lwcell} = 1.028*\delta^{18}O_{cell} - 30.4$ (n = 7; $r^2 = 0.998$; RMSD = 0.2)

The Zhu et al. (2014) aquatic moss calibration dataset is smaller than the van Hardenbroek et al. (2018) dataset for subfossil chironomid head capsules in terms of the number of lakes, spatial

315 extent, and the range of $\delta^{18}O$ values. The Zhu et al. (2014) field sites are all located in southern
316 Patagonia and contain a variety of species (which show some fractionation differences), with
317 modern lake water $\delta^{18}O$ values ranging from -14.3 to -3.8‰. Evidence for a noticeable
318 temperature influence on the fractionation between cellulose and lake water has been
319 demonstrated in the past (Sternberg and Ellsworth, 2011). Analytical precision of the $\delta^{18}O$ values
320 is ±0.4‰. The combined analytical uncertainty and lake water regression uncertainty for
321 $\delta^{18}O_{lwmoss}$ and $\delta^{18}O_{lwcell}$ is ±0.5‰.

322 To loosely constrain the temperature change that may be reflected in $\delta^{18}O_{lw}$ shifts at Lake
323 N14 (which would also have been influenced by changes in precipitation seasonality and
324 moisture source/path) requires knowledge of the complex relationship between temperature and
325 isotopes of precipitation in south Greenland at the YD-Holocene transition. We investigated the
326 applicability of a paleothermometer coefficient (Sime et al., 2019) from GISP2 for the YD-
327 Holocene transition (Buizert et al., 2014) by comparing it to our own calculations of
328 paleothermometer coefficients for the same time period at DYE3 and south Greenland
329 (Narsarsuaq/Lake N14). The nearby GISP2 paleothermometer coefficient was calculated by
330 Buizert et al. (2014) using the ice core $\delta^{18}O$ shift from the YD to Holocene and an independent
331 $\delta^{15}N\text{-}N_2$ GISP2 temperature estimate (~0.33‰ / °C). Importantly, the paleothermometer
332 coefficient varies through space and time (Buizert et al., 2014) because it incorporates the effects
333 of changing moisture sources and seasonality, hence the need to test the applicability of the
334 GISP2 paleothermometer coefficient to our study site. We further describe how we estimated the
335 DYE3 and local paleothermometer coefficient at Lake N14 to validate the use of the YD ~0.33‰
336 / °C paleothermometer coefficient in the discussion section. These YD paleothermometer
337 coefficients are very different from the estimated modern value over Greenland of ~0.7‰ / °C

(Dansgaard et al., 1964), most likely due to differences in moisture source/path and precipitation seasonality in the YD compared to the present (Alley, 2000; Buizert et al., 2014).

4. Results

4.1 Age-Depth Model

Our age-depth model for core 19-N14-N7 (350-240 cm total sediment depth) is based on 24 radiocarbon ages (Fig. 3; Table 1). The dated sediments span ~13,600-8000 cal yr BP, with an additional constraint of -69 cal yr BP assumed for the top of the full three-section core (i.e., 0 cm total sediment depth). The lowermost radiocarbon date at 341 cm has an age of 13,605 (13,480-13770; 2σ) cal yr BP. From 340-325 cm, the sedimentation rate is relatively low (0.01 cm/yr). From 325-260 cm, the sedimentation rate is higher (0.03 cm/yr) and stable but decreases abruptly from 260-255 cm (0.005 cm/yr) before returning to higher values again from 255-200 cm (0.03 cm/yr). Near the base of the core, little material was available for radiocarbon dating, which necessitated the submission of very small macrofossil and bulk sediment samples. Three of the small plant macrofossil samples resulted in calibrated ages that were too young and one of the bulk sediment ages resulted in a calibrated age that was too old (Fig. 3). These were included in the Bacon age-depth model but were excluded as outliers for the calculation of the mean age.

355

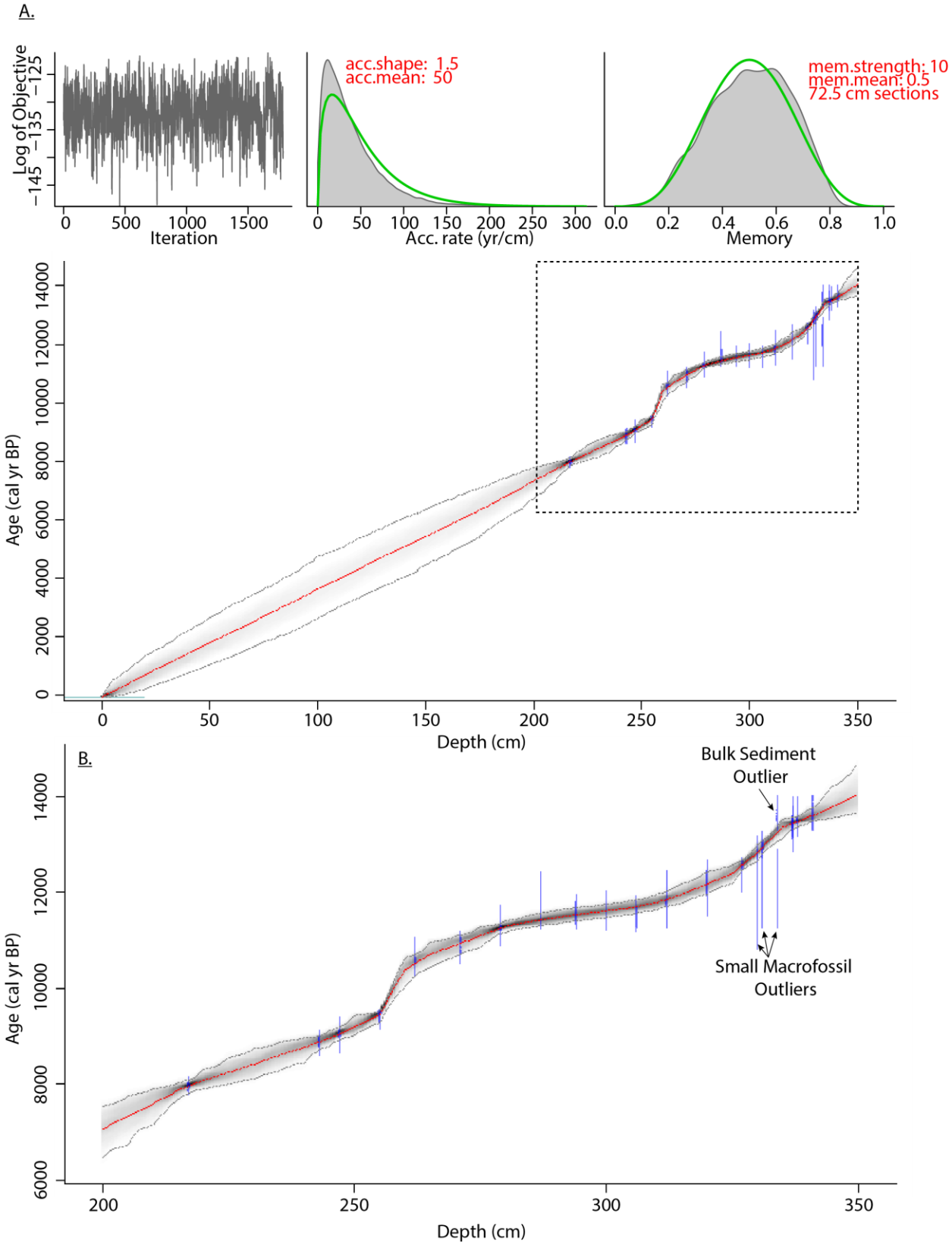
A.
Log of Objective
−145
−135
−125
0
500
1000
1500
Iteration
acc.shape: 1.5
acc.mean: 50
0
50
100
150
200
250
300
Acc. rate (yr/cm)
mem.strength: 10
mem.mean: 0.5
72.5 cm sections
0.0
0.2
0.4
0.6
0.8
1.0
Memory
Age (cal yr BP)
0
2000
4000
6000
8000
10000
12000
14000
0
50
100
150
200
250
300
350
Depth (cm)
B.
Bulk Sediment
Outlier
Small Macrofossil
Outliers
Age (cal yr BP)
6000
8000
10000
12000
14000
200
250
300
350
Depth (cm)

356

Fig. 3 (A) The full 19-N14-N7 age-depth model. The top three small figures (from left to right) show the Markov Chain Monte Carlo iterations, and the prior (green lines) and posterior densities (grey shaded areas) for the accumulation rate and memory. Below, blue shapes are the calibrated radiocarbon ages (n=24). The red line is the mean age. The edge of the gray cloud indicates the 95% confidence interval. Age model assumes -69 cal yr BP at 0 cm sediment depth. The dashed box in the age-depth model indicates the extent of panel B. (B) The lower portion of the 19-N14-N7 age-depth model (Medeiros et al., 2022). Arrows point to the outlier age-depth tie points discussed in the text.

Table 1 Radiocarbon ages and calibrated age results from 19-N14-N7 (Medeiros et al., 2022). Aquatic moss samples with an asterisk were relatively small and resulted in ages that are too young for their depth. The sediment organic carbon sample with an asterisk resulted in an age too old for its depth.

Sample ID	Core Depth (cm)	Material	F Modern	^{14}C Age (^{14}C yr BP)	^{14}C Age Error (2σ)	Median Cal. Age (cal yr BP)	Min. Cal. Age (cal yr BP, 2σ)	Max. Cal. Age (cal yr BP, 2σ)
NOSAMS 162389	217	Aquatic Moss	0.4107	7150	35	7970	7875	8020
NOSAMS 163563	243	Aquatic Moss	0.3694	8000	35	8870	8655	9005
NOSAMS 162390	247	Aquatic Moss	0.3645	8110	35	9055	8985	9260
NOSAMS 163564	255	Aquatic Moss	0.3491	8450	35	9485	9425	9535
NOSAMS 162391	262	Aquatic Moss	0.3114	9370	45	10590	10435	10710
NOSAMS 163565	271	Aquatic Moss	0.305	9540	45	10890	10695	11095
NOSAMS 163566	279	Aquatic Moss	0.2929	9860	45	11260	11195	11395

NOSAMS 162392	287	Aquatic Moss	0.2852	10100	50	11670	11400	11875
NOSAMS 163567	294	Aquatic Moss	0.2868	10050	45	11565	11340	11810
NOSAMS 163568	300	Aquatic Moss	0.287	10050	55	11565	11325	11815
NOSAMS 163569	306	Aquatic Moss	0.2876	10000	55	11485	11270	11730
NOSAMS 162393	312	Aquatic Moss	0.2829	10150	50	11780	11405	11945
NOSAMS 163570	320	Aquatic Moss	0.2752	10350	60	12205	11940	12475
Beta Analytic 539249	327	Aquatic Moss	0.2699	10520	40	12550	12335	12680
NOSAMS 173090	330	Aquatic Moss*	0.2773	10300	150	12100	11405	12620
NOSAMS 173089	330	Sediment Organic Carbon	0.254	11000	65	12925	12770	13080
NOSAMS 173092	331	Aquatic Moss*	0.2727	10450	120	12325	11940	12700
NOSAMS 173091	331	Sediment Organic Carbon	0.2522	11050	65	12975	12830	13100
NOSAMS 173094	334	Aquatic Moss*	0.2721	10450	120	12325	11940	12700
NOSAMS 173093	334	Sediment Organic Carbon*	0.2316	11750	70	13605	13480	13770
NOSAMS 173095	337	Sediment Organic Carbon	0.236	11600	70	13460	13315	13595
NOSAMS 173097	338	Aquatic Moss	0.2386	11500	110	13370	13170	13585
NOSAMS 173096	338	Sediment Organic Carbon	0.235	11650	70	13510	13335	13735
NOSAMS 173098	341	Sediment Organic Carbon	0.2314	11750	70	13605	13480	13770

370

371 *4.2 Bulk Sediment Characteristics*

The 19-N14-N7 core shows a clear transition zone from a basal unit of massive gray, high-MS, high-Ti minerogenic material to laminated brown-tan sediments with moderately high MS and Ti at ~345.5 cm (Fig. 4). From ~333.5 - 328.5 cm, there is a gray disturbed layer (no MS or XRF data available). Sediments then transition to low-MS, low-Ti, dark brown, moss-rich gyttja at ~328.5 cm. The horizontal stratigraphy appears tilted by coring from ~334 - 328 cm and ~305 - 280 cm but laminations are preserved. The moss-rich gyttja layer transitions to a moss-poor gyttja layer at 255.5 cm. S concentration varies substantially throughout the core but shows relatively low values in the moss-rich gyttja layer from ~328.5 - 310 cm, ~305 - 265 cm, and just above it in the moss-poor gyttja layer from ~255 - 240 cm.

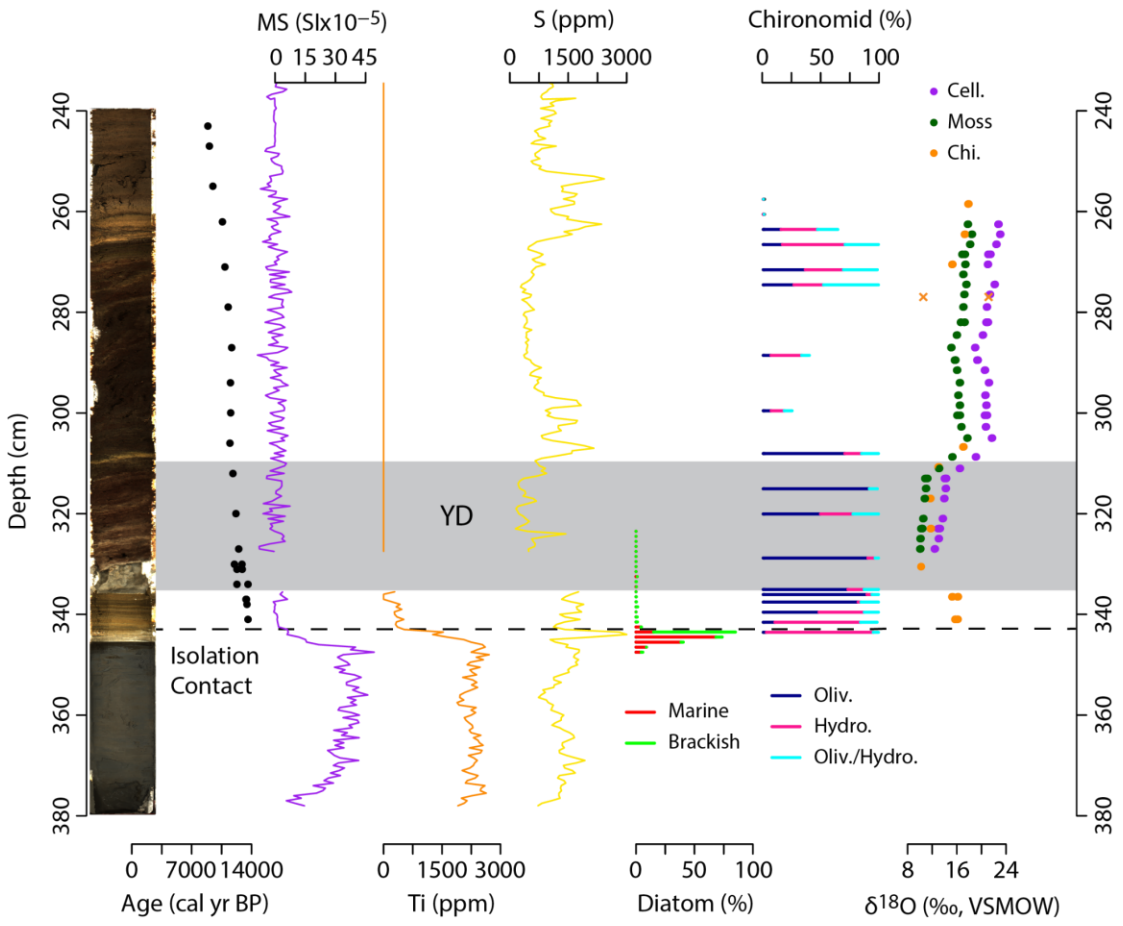

Fig. 4 Core 19-N14-N7 visual stratigraphy, bulk sediment composition, biotic assemblages, and $\delta^{18}O$ of aquatic organic materials. Both y-axes show total sediment depth (cm). From left to right, the data presented includes a core image, calibrated ^{14}C ages (black dots), bulk sediment magnetic susceptibility (MS; purple), titanium (orange), and sulfur (yellow) in bulk sediments, relative abundances of marine and brackish indicator diatom taxa, relative abundances of extreme-cold indicator chironomid taxa (Oliv. = *Oliveridia*, Hydro. = *Hydrobaenus*), and $\delta^{18}O$ of aquatic moss cellulose (cell.), bulk moss (moss), and subfossil chironomid head capsules (chi.). The two orange xs are outlier duplicate $\delta^{18}O$ samples that were removed. The analytical uncertainty of the $\delta^{18}O$ measurements is 0.4‰ and is smaller than the size of the points. Note that elemental concentrations are estimated in ppm but given instrument calibration uncertainties are most useful for relative comparisons. The approximate timing of the YD (based on Lake N14 $\delta^{18}O$ values and supported by ^{14}C ages) is represented by the horizontal gray band. The black dashed line indicates the diatom inferred isolation contact.

4.3 Diatom and Chironomid Assemblages

Diatoms indicate that the isolation contact, when the lake was separated from marine influence, occurs at 13,720 cal yr BP (343.5 cm). An abrupt marine to lacustrine transition is indicated by a shift in diatom indicators from poly- and mesohalobous taxa, dominated by *Navicula digitoradiata*, *Navicula apiculata* and *Trachyneis aspera* to an oligohalobous-indifferent assemblage with abundant *Fragilariaceae*, *Navicula meniscus*, and *Navicula margalithii* above this point (Figs. 4, S1). Subsequent diatom assemblages are dominated by

403 *Fragilariaceae* from this level upwards, through the lower gyttja, unlaminated silt-rich layer and
404 into the moss-rich gyttja above.

405 Chironomid assemblages were analyzed above the isolation contact in 19-N14-N7 and
406 were previously described by Medeiros et al. (2022). Here we summarize the key results
407 pertaining to Younger Dryas climate changes. Head capsule concentrations ranged from >150
408 head capsules g^{-1} (wet sediment) in some sections of Allerød and early Holocene gyttja to <20
409 head capsules g^{-1} in moss-rich sediments of the Younger Dryas and earliest Holocene (Fig. S2).
410 Assemblages in Allerød and Younger Dryas sediments were 96 - 100% composed of varying
411 proportions of the cold stenotherms *Oliveridia* and *Hydrobaenus* (Figs. 4, S2). Late glacial
412 assemblages had closest modern analogs in the high Arctic Archipelago of Canada, though a
413 goodness-of-fit (based on squared residual lengths) to the WA-PLS model was poor for these
414 low-diversity assemblages. Summer temperature anomalies (relative to modern; see Methods)
415 modeled from chironomid assemblages averaged -7.5 to -8°C during the Allerød and -9 °C
416 during the Younger Dryas (Fig. 5). *Oliveridia* and *Hydrobaenus* declined sharply between two
417 samples at the start of the Holocene ~11,600 cal yr BP, as new taxa arrived: *Micropsectra* and
418 *Psectrocladius,* and low abundances of *Einfeldia pagana*-type and *Corynocera oliveri*-type
419 (Figs. 4, S2). The numbers of subfossil head capsules were low (<10) in the earliest part of the
420 Holocene but nonetheless clearly show this major transition in chironomid assemblages (Fig.
421 S2), which suggests rapid climate amelioration (and reconstructed summer temperatures rising
422 ~6°C; Fig. 5) at the end of the Younger Dryas. By 11,100 cal yr BP, the chironomid fauna
423 shifted back to *Hydrobaenus*-dominated assemblages, suggesting a return to cold-water
424 conditions and/or protracted lake ice cover. By ~10,600 cal yr BP, *Einfeldia* and *C. oliveri*-type
425 returned, and the early Holocene period of surprisingly cold conditions began to warm. Cold

stenotherms had disappeared from Lake N14 by ~10,500 cal yr BP, when near-modern summer temperatures are inferred. Subfossil assemblages younger than 10,500 cal yr BP have closest modern analogs in the low arctic climate of southwest Greenland (Medeiros et al., 2022), similar to the modern-day climate at Lake N14.

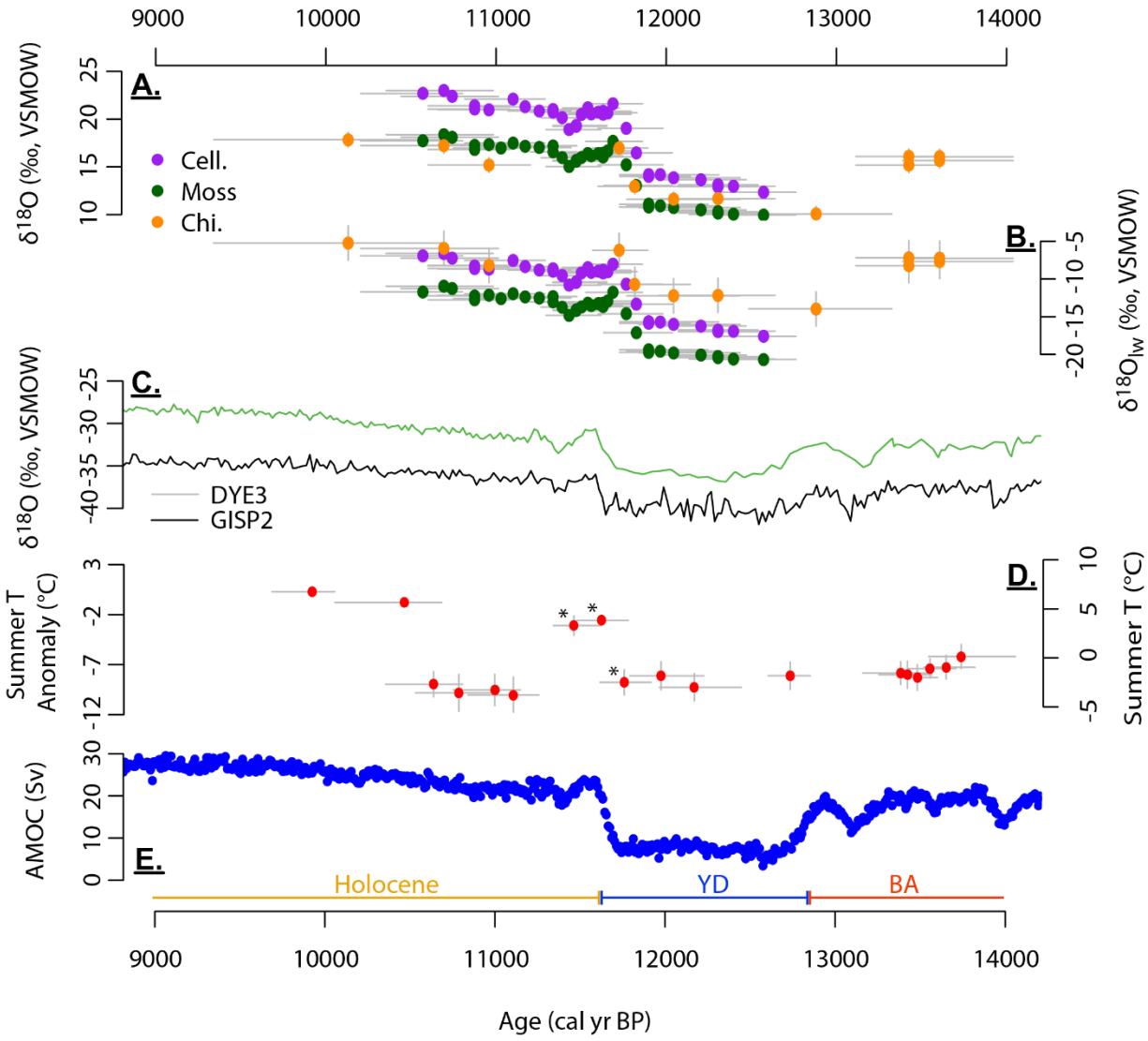

Fig. 5 Local and regional paleoclimate records from ~14,000 - 9000 cal yr BP. (A) Organic material $\delta^{18}O$ values of moss cellulose (purple), bulk moss (green), and chironomid head capsules (orange) from Lake N14 sediment. (B) Lake water $\delta^{18}O$ ($\delta^{18}O_{lw}$) modeled from $\delta^{18}O$

values of moss cellulose, bulk moss, and chironomid head capsules (see methods). The points represent the midpoint age of each sample. The vertical gray uncertainty lines include the analytical uncertainty associated with the $\delta^{18}O$ measurement (for panels A and B) and the uncertainty associated with the regression equations for converting to lake water (for panel B; see methods). These error bars are smaller than the points for all data in panel A and moss and cellulose data in panel B. The horizontal gray lines reflect the age uncertainty in the model associated with the uppermost and lowermost sediment depths of each sample. (C) Ice core $\delta^{18}O$ values from DYE3 (green; Dansgaard et al., 1982; Badgeley et al., 2020) and GISP2 (black; Grootes and Stuiver, 1997; see Fig. 1A for locations). (D) Chironomid assemblage-based summer air temperature anomalies from Lake N14 (via WA-PLS modeling; Medeiros et al., 2022). Starred samples had <50 identified head capsules due to low concentrations. Anomalies were calculated relative to modern species assemblages in surface sediments. (E) Modeled AMOC strength (Sv; 10^6 m^3 s^{-1}) required to bring TraCE-21 K simulations and ice core reconstructions into agreement (Buizert et al., 2018). The basal colored bars indicate the approximate timing of the Holocene (yellow), Younger Dryas (YD; blue), and Bølling-Allerød (BA; red) based on the GISP2 isotope excursions (Rasmussen et al., 2006).

4.4 $\delta^{18}O$ Values and Inferred Temperatures

$\delta^{18}O_{chi}$ values were measured from ~13,600 - 10,100 cal yr BP and range between 11.6 - 17.8‰ (Figs. 4, 5). Modeled lake water oxygen isotope ($\delta^{18}O_{lwchi}$) values range from -14.0 to -5.2‰ (Fig. 5). Average $\delta^{18}O_{lwchi}$ values for the early Holocene, YD, and BA are -6.4 (n = 4), -12.3 (n = 4), and -7.6‰ (n = 4), respectively. The BA-YD transition occurred between ~13,450 -

12,900 cal yr BP based on $\delta^{18}O_{lwchi}$ values and the age-depth model. The YD-Holocene transition at the center of the rise of $\delta^{18}O_{lwchi}$ values dates to ~11,750 cal yr BP. $\delta^{18}O_{lwchi}$ values increase slightly through the early Holocene (~1‰ from 11,700 to 10,100 cal yr BP). Additionally, we present a modern calibration point with a surface sediment (0-2 cm) $\delta^{18}O_{chi}$ value of 13.1 ± 0.4‰. After using Equation 1, we reconstruct a $\delta^{18}O_{lwchi}$ value of -10.6 ± 2.3‰. Within uncertainties, this overlaps with measured August 2019 lake water $\delta^{18}O$ (-8.3 ± 0.3‰; n = 3; Fig. 2D) and is very close to an estimate of mean annual precipitation $\delta^{18}O$ using amount weighted (based on modern Qaqortoq precipitation amounts) monthly isotope values (Bowen, 2022; Bowen et al., 2005; IAEA/WMO, 2015) of -10.5‰.

$\delta^{18}O_{moss}$ values were measured from ~12,600 - 10,600 cal yr BP and range from 10.0 - 18.4‰ (Figs. 4, 5). $\delta^{18}O_{cell}$ values were measured over the same time interval and range from 12.3 - 23.0‰ (Figs. 4, 5). $\delta^{18}O_{lwmoss}$ values range from -20.7 to -11.0‰ and $\delta^{18}O_{lwcell}$ values range from -17.6 to -6.6‰ (Fig. 5). Average $\delta^{18}O_{lwmoss}$ values for the early Holocene and YD are -12.8 (n = 24) and -20.0‰ (n = 9), respectively. Average $\delta^{18}O_{lwcell}$ values for the early Holocene and YD are -8.7 (n = 23) and -16.4‰ (n = 9), respectively. The timing of the YD-Holocene transition based on the center of the rise of $\delta^{18}O_{lwmoss}$ and $\delta^{18}O_{lwcell}$ values is also ~11,750 cal yr BP. $\delta^{18}O_{lwcell}$ and $\delta^{18}O_{lwmoss}$ values show parallel decreases of 2.5 and 2.0‰, respectively, at ~11,550 - 11,350 cal yr BP. $\delta^{18}O_{lwmoss}$ and $\delta^{18}O_{lwcell}$ values increase slightly through the early Holocene (~1 - 2‰; 11,350 - 10,600 cal yr BP).

To assess whether the paleothermometer coefficient derived at GISP2 for the end of the YD (0.33‰ / °C ; Buizert et al., 2014) was reasonable to apply to our site in southern Greenland, we compared the mean YD (n=4) to Holocene (n=4) shift at Lake N14 $\delta^{18}O_{lwchi}$ (5.9 ± 2.3‰) to a $\delta^{18}O$-independent reconstruction of annual temperature change in south Greenland (Narsarsuaq

to the southern tip of Greenland) that is based upon ice core $\delta^{15}N$ data combined with climate model-based estimates of past seasonality and spatial patterns in temperature (~18.3°C; Buizert et al., 2018). This yielded a paleothermometer coefficient of ~0.33‰ / °C for south Greenland/Lake N14 at the YD-Holocene transition. Using this same approach with DYE3 $\delta^{18}O$ values at the YD-Holocene transition (~4.4‰; Dansgaard et al., 1982; Badgeley et al., 2020) and an independent $\delta^{15}N$ data/modeled temperature reconstruction of the YD-Holocene transition at DYE-3 (~13.3°C; Buizert et al., 2018), we calculated essentially the same paleothermometer coefficient of ~0.33‰ / °C for this time period at DYE-3, supporting the applicability of this value across a broad area of central to southern Greenland at the end of the YD.

We used $\delta^{18}O_{lwchi}$ values to estimate annual temperature changes at the end of the YD because chironomids have a large modern dataset for understanding their biosynthetic fractionation in the Arctic and no evidence of species-specific vital effects. Applying the paleothermometer coefficient discussed above suggests a YD-Holocene temperature increase of 17.8 ± 7.0°C. This should be considered a rough estimate.

5. Discussion

5.1 Performance and Interpretation of $\delta^{18}O$ Proxies

Here, we first evaluate reconstructions of lake water $\delta^{18}O$ ($\delta^{18}O_{lw}$) and thus precipitation $\delta^{18}O$ from the $\delta^{18}O$ of the three different organic materials analyzed for their oxygen isotopic composition downcore. We assess the possible influences of temperature-dependent biosynthetic fractionations and of changes in seawater $\delta^{18}O$ on our resulting reconstructions of precipitation

500 $\delta^{18}O$. Next, we discuss the potential for precipitation $\delta^{18}O$ reconstructions to be influenced by
501 changes in elevation, moisture source/path, precipitation seasonality, and temperature.

502 $\delta^{18}O_{moss}$ and $\delta^{18}O_{cell}$ track each other in remarkable parallel way across the YD and early
503 Holocene (Fig. 5), but with $\delta^{18}O_{cell}$ values 3.8 ± 1.2‰ higher than $\delta^{18}O_{moss}$. This offset is much
504 larger than the offset of ~1‰ described by Zhu et al. (2014) based on samples from several
505 Patagonian lakes. Some potential explanations for this offset include the differences between the
506 pretreatment protocols to remove potential inorganic contaminants, cellulose extraction
507 techniques, and/or the species of moss. Because of these differences, we have less confidence in
508 the absolute values of the $\delta^{18}O_{lwmoss}$ curve that was generated using the regression developed by
509 Zhu et al. (2014) compared to the $\delta^{18}O_{lwchi}$ and $\delta^{18}O_{lwcell}$ values. However, the parallel trends of
510 $\delta^{18}O$ in the two materials supports that both are reliably recording changes in the same
511 environmental parameter, namely $\delta^{18}O_{lw}$. Likewise, chironomid $\delta^{18}O$ trends closely parallel
512 trends in moss and cellulose $\delta^{18}O$ where the two materials are both preserved (Fig. 4), supporting
513 that chironomids are also recording $\delta^{18}O_{lw}$.

514 Interestingly, the absolute values of $\delta^{18}O_{lwchi}$ and $\delta^{18}O_{lwcell}$ are similar in the early
515 Holocene but diverge in the YD (Fig. 5). One potential explanation for this deviation could be
516 different temperature sensitivities of isotope fractionation for cellulose versus chitin
517 biosyntheses. Evidence has suggested that both $\delta^{18}O_{chi}$ and $\delta^{18}O_{cell}$ values are influenced by the
518 temperature of the host water during biosynthesis and at different magnitudes (Sternberg and
519 Ellsworth, 2011; Lombino et al., 2021). To investigate the potential impact of this effect during
520 the YD-Holocene transition, we reconstructed YD $\delta^{18}O_{lw}$ values with the temperature dependent
521 regression lines and an assumed summer temperature increase at the YD-Holocene transition of
522 ~6°C based on chironomid assemblages (Fig. 5). We use the summer temperature reconstruction

because aquatic mosses and possibly chironomid larvae grow most in the summer (Oliver, 1968). This temperature reconstruction will, therefore, provide a reasonable method for assessing the impact of the temperature effect on $\delta^{18}O_{lwchi}$ and $\delta^{18}O_{lwcell}$ at the YD-Holocene transition. To infer the change in $\delta^{18}O_{lwchi}$ based on a temperature dependent fractionation, we used Equation 4:

(4) $\Delta_{chironomidl\text{-}lw} \approx 1000 \cdot \ln\alpha^{18}O_{chironomid-lw} = 6.29 * (1000 / (T+273.15)) + 1.16$ ($r^2 = 0.66$; $p < 0.05$; $n = 8$)

Where $1000 \cdot \ln\alpha^{18}O_{chironomid-lw}$ is the fractionation of $(^{18}O/^{16}O)_{chi}$ relative to $(^{18}O/^{16}O)_{lw}$ and T is temperature in degree Celsius (Lombino et al., 2021).

To infer the change in $\delta^{18}O_{lwcell}$ based on a temperature-dependent fractionation, we used Equation 5:

(5) $1000 \cdot \ln\alpha^{18}O_{chironomid-lw} \approx \Delta_{cell\text{-}lw} = 0.0073T^2 - 0.4375T + 32.528$ ($r^2 = 0.829$; $p < 0.05$; $n = 13$)

Where $\Delta_{cell\text{-}lw}$ is the enrichment of $^{18}O_{cell}$ relative to $^{18}O_{lw}$ and T is temperature in degree Celsius (Sternberg and Ellsworth, 2011).

Upon comparing the results of $\delta^{18}O_{lwchi}$ and $\delta^{18}O_{lwcell}$ derived from the above temperature-dependent fractionation equations with the non-temperature-dependent fractionation equations (see methods), we observed that the temperature dependent fractionation would cause the magnitude of $\delta^{18}O_{lwchi}$ and $\delta^{18}O_{lwcell}$ shifts at the YD-Holocene transition to increase by ~0.1 and ~1.9‰, respectively. This appears to indicate that chironomid chitin is less impacted by temperature dependent fractionation than aquatic moss cellulose in this temperature range. Thus, taking the potential host water temperature fractionation effect at this site into account would

likely increase the differences between estimated $\delta^{18}O_{lwchi}$ and $\delta^{18}O_{lwcell}$ values and the inferred temperature changes, rather than making them more similar.

Over the deglacial period, the $\delta^{18}O$ value of seawater decreased as total glacial ice volume decreased. To investigate the impact a change in the $\delta^{18}O$ values of seawater would have on precipitation $\delta^{18}O$ values (and therefore our lake water proxies) during the YD, we use Equation 6 (Stenni et al., 2010; Porter et al., 2019):

$$(6)\ \delta^{18}O_{corr} = \delta^{18}O_{lw} - \delta^{18}O_{sw} * (1 + \delta^{18}O_{lw} / 1000)/ (1 + \delta^{18}O_{sw} / 1000)$$

Where $\delta^{18}O_{corr}$ is the seawater corrected proxy $\delta^{18}O_{lw}$ value ($\delta^{18}O_{lwchi}$, $\delta^{18}O_{lwmoss}$, or $\delta^{18}O_{lwcell}$) and $\delta^{18}O_{sw}$ is the change in seawater $\delta^{18}O$ relative to modern that is only attributable to changes in ice volume (temperature corrected; Rohling et al., 2021). These temperature corrected seawater $\delta^{18}O$ values linearly decreases by ~0.3‰ from 13,500-10,100 cal yr BP. We find that using this correction causes the shifts in our proxies at the start and end of the YD to change by <0.1‰ (well within uncertainty of measurement) and therefore has little influence on our climatic interpretations at these times. However, the correction does cause the absolute $\delta^{18}O_{lw}$ values to decrease by around 0.1 - 0.5‰ (with a greater decrease at the YD onset), relevant to comparing YD values with modern.

Precipitation $\delta^{18}O$ values inferred from our record in south Greenland can be compared directly with $\delta^{18}O$ values from ice cores recovered from the Greenland Ice Sheet to assess spatial patterns in isotopes of precipitation. The elevations of Lake N14 and the Greenland ice core sites presently differ by ~2400 (DYE3) and 3200 m (GISP2), which causes the absolute values of precipitation $\delta^{18}O$ values to differ, rather than the magnitude of the shifts at the start and end of the YD. Over longer timescales, gradual elevation change at Lake N14 due to isostatic rebound

566 and lowering of the ice core sites through time would influence the comparison of precipitation
567 $\delta^{18}O$ shifts between sites. In general, a reduction in the elevation across the Greenland Ice Sheet
568 would increase the magnitude of warming or suppress the magnitude of cooling suggested by
569 $\delta^{18}O$ shifts.

570 YD climate shifts involved changes in moisture sources, seasonal amounts of
571 precipitation, and temperature, all of which affect the $\delta^{18}O$ values of precipitation. Much of the
572 modern moisture that falls as precipitation in south Greenland originates from the North Atlantic,
573 the Great Lakes region, Hudson Bay, and the eastern coast of North America (Nusbaumer et al.,
574 2019). Renssen et al. (2015) modeled major changes in atmospheric circulation in addition to
575 ocean circulation associated with the YD. Additional evidence from ice, lacustrine sediment, and
576 marine sediment cores suggests that storm tracks around Greenland moved southward at the
577 onset of the YD and northward at the end of the YD (Mayewski et al., 1993; Kapsner et al.,
578 1995; Bakke et al., 2009). The southward movement of the polar front at the YD onset was most
579 likely related to expanded sea ice cover as a result of reduced North Atlantic Deep Water
580 formation and reduced AMOC driven poleward transport of equatorial heat (Fig. 5E; Kapsner et
581 al., 1995; Bakke et al., 2009). At the end of the YD, the polar front and sea ice cover likely
582 moved northwards (Dansgaard et al., 1989; Bakke et al., 2009), opening the nearby North
583 Atlantic as a potential moisture source for Lake N14. More precipitation from the nearby North
584 Atlantic in the early Holocene would increase $\delta^{18}O_{lw}$ values relative to more distal sources
585 during the YD.

586 Major movement of storm tracks would also influence the total amount of precipitation
587 and precipitation seasonality at Lake N14. Central Greenland ice core records suggest snow
588 accumulation doubled at the YD-Holocene transition (Alley, 2000). This snow accumulation

589 change was likely driven by increases in air temperature and movement of storm tracks closer to
590 Greenland at the end of the YD (Fawcett et al., 1997; Alley, 2000). The greatest increase in
591 precipitation amount at the YD-Holocene transition was likely in the winter season (Fawcett et
592 al., 1997; Alley, 2000) due to a strengthening AMOC increasing winter temperatures and
593 reducing sea ice cover (Fig. 5E; Alley, 2000). Additionally, GCMs indicate that precipitation
594 seasonality changes were greater in south Greenland compared to central and northern Greenland
595 for the YD (Buizert et al., 2014). The changes in moisture source/path and precipitation
596 seasonality that are described above cause the (separately calculated) GISP2, DYE3, and Lake
597 N14 YD-Holocene paleothermometer coefficients (~0.33‰/°C) to be smaller than the modern
598 spatial value over Greenland (~0.7‰ / °C; Dansgaard, 1964). The smaller coefficient value
599 reflects altered influence of non-temperature effects like moisture source/path and precipitation
600 seasonality compared to the present (Buizert et al., 2014; Badgeley et al., 2020). Precipitation
601 $\delta^{18}O$ shifts reflect changes in moisture source/path, precipitation seasonality, and temperature;
602 and because the calculations of these paleothermometer coefficients use an independent $\delta^{15}N$-
603 based method to estimate paleotemperatures, these coefficients intrinsically incorporate the
604 altered non-temperature effects on precipitation $\delta^{18}O$ values. The similarity of the independently
605 derived GISP2, DYE3, and Lake N14/south Greenland paleothermometer coefficients at the end
606 of the YD suggest that 1) this value is reasonable to use at Lake N14 for the YD-Holocene
607 transition and 2) the net precipitation isotope effects from shifts in moisture source/path and
608 precipitation seasonality may have been similar for the YD-Holocene across central and southern
609 Greenland. Nonetheless, our estimates here of temperature change based upon $\delta^{18}O$ values must
610 be viewed as tentative, given that there were undoubtedly some spatial differences in these

effects between central and southern Greenland and paleotemperature coefficients were derived from data with quite large uncertainties.

5.2 Early Isostatic Emergence of Lake N14 Confirmed

Coastal Greenland sites like Lake N14 are useful for reconstructing relative sea level (RSL) changes and regional ice sheet history. Indeed, Lake N14 is the earliest documented emergence of a Greenland lake during the last deglaciation. Previous research found that isostatic rebound led to the isolation of the lake from a former marine basin at ~13,800 cal yr BP (Bennike and Björck, 2000; Bennike et al., 2002, Björck et al., 2002). This timing was based on a radiocarbon age from terrestrial moss collected across the 6 cm directly above the isolation contact (recalibrated to ~13,530 cal yr BP using Calib 8.2 and IntCal20; Bennike and Björck, 2000; Björck et al., 2002). Upon revisiting this site ~20 years later, we found the same transition from a high-MS, mineral-rich massive gray marine unit containing no lacustrine insect remains to a lower-MS, laminated light brown lacustrine unit preserving abundant lacustrine chironomids (sedimentological isolation contact at 345.5 cm; Fig. 4). We use diatom analysis to precisely pinpoint the lake's isolation at 343.5 cm (diatom-inferred isolation contact; Fig. 4). A sulfur peak is also coincident with the isolation process (345.5 - 343.5 cm; Fig. 4), which is expected from anoxic bottom water and sulfur reducing conditions (Long et al., 2011). We estimate the timing of the diatom-inferred isolation contact to be 13,675 (13,560-13,780; 2σ) cal yr BP based on the age model created for the bottom section of the core (Fig. 4). The deepest radiocarbon age we obtained was 13,605 (13,480-13770; 2σ) cal yr BP at 341 cm (Table 1). We therefore report this as a minimum age for local ice-free conditions and confirm that pre-YD lacustrine sediment is

present in Lake N14. The timing of isolation agrees with Björck et al. (2002) who suggested basin isolation occurred at ~13,800 cal yr BP. It also agrees with Levy et al. (2020), who concluded that south Greenland deglaciated earlier than southeast Greenland due to relatively high BA temperatures, low precipitation amounts, and deeper and wider fjords (which decrease glacial drag and enhance the incursion of warm water). RSL continued to fall after the isolation of Lake N14 (33 m a.s.l.), with the next recorded lake isolation (Lake N18, 30 m a.s.l.), 14 km east around 11,900 cal yr BP (Bennike et al., 2002). The new dates confirm that N14 is the earliest deglacial lake isolation reported from Greenland, and was followed by relatively slow RSL fall in this region between ~13,700 - 11,900 cal yr BP at a rate of ~1.6 mm/yr. This suggests slow rates of mass loss compared to the early Holocene when RSL fall was closer to 20 mm/yr (Bennike et al., 2002).

5.3 Younger Dryas Climate

Our $\delta^{18}O_{lwchi}$, $\delta^{18}O_{lwmoss}$, and $\delta^{18}O_{lwcell}$ data suggest that southernmost Greenland experienced greater climate changes at the end of the YD compared to the GISP2 and DYE3 $\delta^{18}O$ records, likely as a result of the closer proximity of Lake N14 to a locus of North Atlantic Deep Water formation in the Labrador Sea (Fig. 5). At the end of the YD, AMOC grew in strength and facilitated the movement of equatorial heat to this location (Fig. 5E). At our site, $\delta^{18}O_{lwchi}$ increased by 5.9‰, $\delta^{18}O_{lwmoss}$ increased by 7.2‰, and $\delta^{18}O_{lwcell}$ increased by 7.7‰ at the end of the YD (Fig. 5), while DYE3 $\delta^{18}O$ values increased by 5.0‰ and GISP2 $\delta^{18}O$ values increased by 3.5‰ (Fig. 5). Annual temperature changes likely explain much of the YD-Holocene shifts in Lake N14 $\delta^{18}O_{lw}$ values in combination with changing seasonal amounts and

$\delta^{18}O$ values of precipitation driven by altered moisture source/path. The combined ice core $\delta^{15}N$ proxy and modeling approach used by Buizert et al. (2018) also indicates a clear latitudinal trend across Greenland, with south Greenland exhibiting the largest modeled temperature changes at the YD-Holocene transition. They propose this is due to reduced equatorial heat transfer to the poles following weakened North Atlantic Deep Water formation and AMOC (Fig. 5E; Buizert et al., 2018). Our results reinforce the idea that YD changes in moisture source/path, precipitation seasonality, and temperature around Greenland were driven by AMOC and most intense in the northwest North Atlantic.

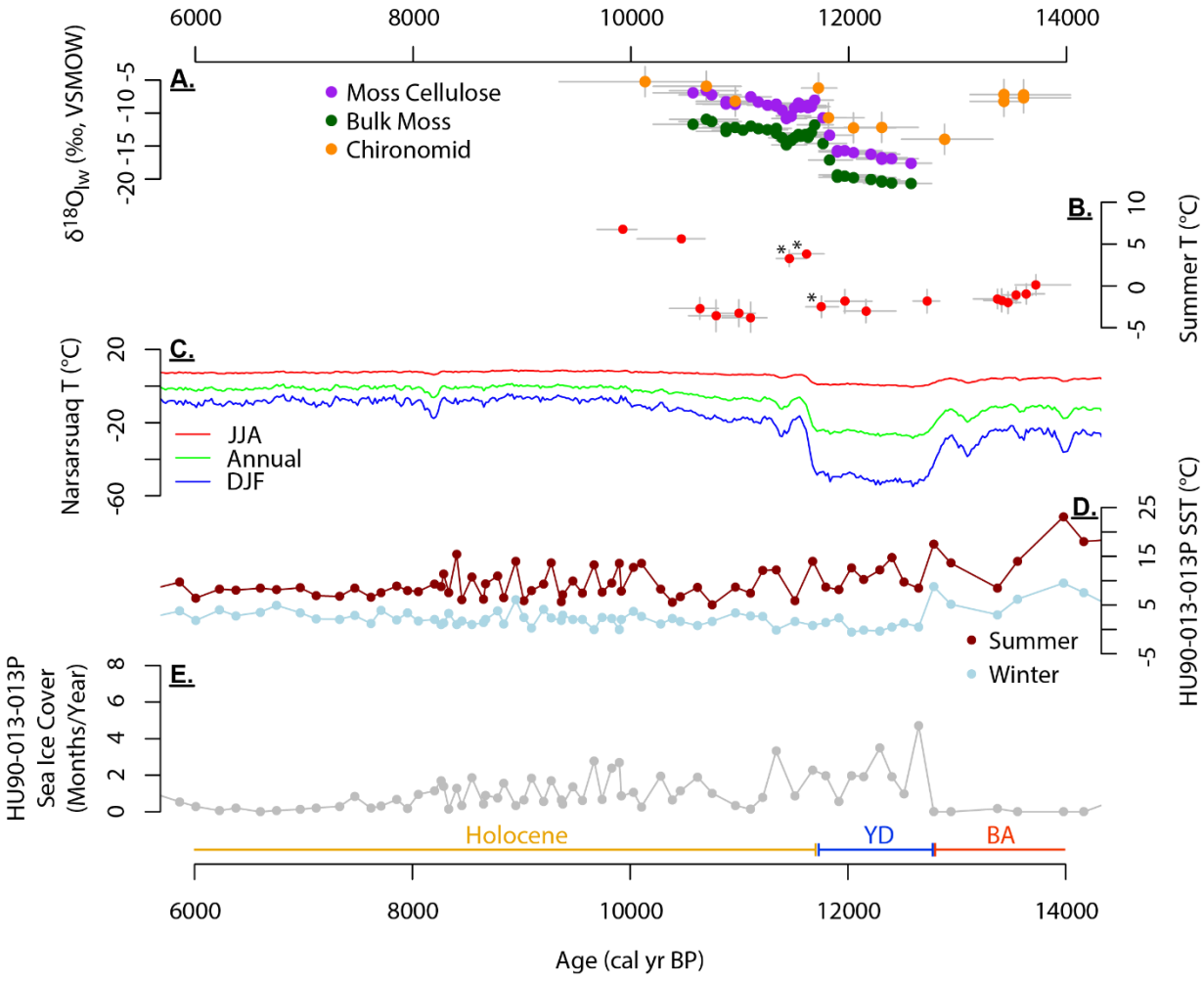

Fig. 6 Lake N14 records compared to regional climate records from ~14,000 - 6000 cal yr BP. (A) Lake water $\delta^{18}O$ ($\delta^{18}O_{lw}$) modeled from $\delta^{18}O$ values of moss cellulose, bulk moss, and chironomid head capsules at Lake N14. Points represent midpoint age of each sample. Vertical gray lines include analytical uncertainty and uncertainty from regression equations for converting to $\delta^{18}O_{lw}$. Uncertainties are smaller than the plotted points for moss and cellulose data. Horizontal gray lines reflect age uncertainty in the model associated with the uppermost and lowermost sediment depths of each sample. (B) Chironomid assemblage-based summer air temperature from Lake N14 (via WA-PLS modeling; Medeiros et al., 2022). Starred samples had <50 identified head capsules due to low concentrations. In some cases, uncertainty is smaller than the size of points. (C) Seasonally resolved modeled temperatures from Narsarsuaq to the southern tip of Greenland (Buizert et al., 2018). (D) Seasonally resolved sea surface temperatures from core HU90-013-013P off the coast of south Greenland (Solignac et al., 2004; de Vernal and Hillaire Marcel, 2006). (E) Months of sea ice cover per year (with 50% sea ice concentration or greater) based on core HU90-013-013P (gray). Basal colored bars indicate the approximate timing of the Holocene (yellow), Younger Dryas (YD; blue), and Bølling-Allerød (BA; red) based on the chronology in Rasmussen et al. (2006).

There is some evidence around south Greenland for expanded sea ice cover during the YD. During this time, sulfur concentrations in Lake N14 sediment were relatively low (Fig. 4), which is consistent with the conclusions of Björck et al. (2002) that sea spray was limited due to sea ice cover based on chemical and diatom evidence. An absence of marine dinoflagellates in YD sediments from coastal Lake N23 (~10 km N/NE of Lake N14) also indicates limited sea spray due to enhanced sea ice cover (Ljung and Björck, 2004). Marine sediment core HU90-013-

687 013P (58°12.59'N, 48°22.40'W; ~270 km southwest of Lake N14) suggests that sea ice cover
688 ranged from 1-5 months per year in the YD based on dinoflagellate cyst assemblages (Fig. 6;
689 Solignac et al., 2004; de Vernal and Hillaire-Marcel, 2006). This is longer sea ice cover than
690 before and after the YD and compared with zero months per year at the core site today.
691 However, it does not suggest near total sea ice cover year-round in the YD, as possibly suggested
692 by the lacustrine proxies. One potential driver of enhanced nearshore sea ice cover in the YD
693 was likely related to the high volume of freshwater flowing into the North Atlantic during
694 deglaciation (Carlson et al., 2007; Leydet et al., 2018), which is thought to have driven AMOC
695 slowdown (McManus et al., 2004). Icebergs and meltwater from the receding Greenland Ice
696 Sheet would have contributed to low sea-surface salinity nearshore around Lake N14 and are
697 inferred from core HU90-013-013P during the YD (Solignac et al., 2004; de Vernal and Hillaire-
698 Marcel, 2006). Low sea-surface salinity could enhance the formation of sea ice. Additionally,
699 there was a relatively large seasonal difference in sea-surface temperatures during the YD, with
700 summer temperatures often greater than 10°C while winter temperatures were around 0°C (Fig.
701 6; Solignac et al., 2004; de Vernal and Hillaire-Marcel, 2006). This is consistent with enhanced
702 seasonality being a key feature of the YD (Denton et al., 2005).

703 Chironomid assemblages lend further support to an increase in seasonality during the YD
704 and a decline in seasonality at the start of the Holocene. The chironomid-inferred summer
705 temperature depression during the YD was 9 - 10 °C relative to modern, larger than the YD
706 summer temperature depression suggested by Denton et al. (2005) based upon a moraine record
707 and inferred glacier equilibrium line altitude changes in East Greenland. This summer cooling
708 during the YD may have been enhanced in south Greenland by proximity to major changes in
709 Labrador Sea surface conditions associated with AMOC slowdown and reduced poleward heat

transport (Fig. 5E). Chironomid-inferred summer temperatures indicate a ~6°C summer temperature increase at the end of the YD, which is modest compared with ~18°C of annual warming tentatively inferred from $\delta^{18}O_{lw}$ at Lake N14 and compared with inferred annual warming at GISP2 or DYE-3. Together, chironomid assemblages and $\delta^{18}O_{lw}$ at Lake N14 support both the long-standing hypothesis of increased seasonality during the YD (Björck et al., 2002; Denton et al., 2005), and the notion of stronger YD climate change over south Greenland than over other parts of Greenland (Buizert et al., 2018) and indeed almost anywhere else in the world.

YD summer (~June-July-August) temperatures inferred from chironomid assemblages were below freezing, suggesting very cool summers, short ice-free seasons, and/or strong suppression of lake water temperatures, akin to modern-day lakes in the coldest high arctic environments today (Gajewski et al., 2005). Björck et al. (2002) highlighted high algal productivity during the YD at Lake N14 and inferred a combination of mild summers and arid conditions, which they posited led to lowered lake level and warmer, more alkaline lake waters and evaporative concentration of nutrients. However, enhanced evaporation of lake water in the YD is not supported by the strongly depleted YD $\delta^{18}O_{lw}$ values at Lake N14. Moreover, chironomids suggest a harsh summer climate and short ice-free season. High alkalinity is common in Arctic lakes occupying freshly deglaciated landscapes (Law et al., 2015). Greater light penetration through lake ice due to reduced YD snow cover also may have helped mitigate the impacts of short ice-free seasons on the lake's primary producers (Riis et al., 2010).

5.4 Early Holocene Climate

One conspicuous feature of the early Holocene at Lake N14 is a brief but significant multi-century decline in $\delta^{18}O_{lw}$ shortly after the onset of the Holocene. The Preboreal Oscillation has been shown in Greenland ice core $\delta^{18}O$ records (Rasmussen et al., 2007) and in diatom assemblage reconstructions from Lake N14 (Björck et al., 2002), but has not been clearly demonstrated in Greenland lake sediment derived $\delta^{18}O$ records due to the need for high-resolution sampling across the earliest Holocene. Our high resolution $\delta^{18}O_{lwmoss}$ and $\delta^{18}O_{lwcell}$ records from Lake N14 show clear parallel decreases of 2 - 3‰ from ~11,550 - 11,350 cal yr BP (Fig. 5), roughly coincident with the timing and duration of the Preboreal Oscillation as previously described elsewhere around the North Atlantic region (Björck et al., 1997, Rasmussen et al., 2007; Fiłoc et al., 2018). The duration and magnitude of the $\delta^{18}O_{lwmoss}$ and $\delta^{18}O_{lwcell}$ shifts are similar to shifts in the DYE3 $\delta^{18}O$ record (Fig. 5; Dansgaard et al., 1982; Badgeley et al., 2020). The onset of the $\delta^{18}O$ decrease at Lake N14 dates 100 - 200 years earlier than ice cores suggest, but that difference in timing falls within our age model's uncertainty. These results reinforce that the $\delta^{18}O$ values of bulk moss and cellulose at Lake N14 record regional precipitation $\delta^{18}O$ and that these proxies can be used to examine short-lived climatic events. The magnitude of $\delta^{18}O_{lwmoss}$ and $\delta^{18}O_{lwcell}$ changes are slightly larger than those recorded by the GISP2 $\delta^{18}O$ record (Fig. 5), potentially indicating there may be a latitudinal variation in the magnitude of Preboreal Oscillation climate change due to the distance from AMOC influences in the North Atlantic (Buizert et al., 2014; Buizert et al., 2018).

Our $\delta^{18}O_{lw}$ reconstructions show increasing trends from 11,400 - 10,100 cal yr BP in south Greenland, much like the GISP2 and DYE3 $\delta^{18}O$ records (Fig. 5; Dansgaard et al., 1982; Grootes and Stuiver, 1997; Badgeley et al., 2020). Over the 11,400 - 10,100 cal yr BP interval, ice core $\delta^{15}N$ data and modeling suggest that annual temperatures increased by ~9°C in

755 southernmost Greenland (Buizert et al., 2018). Ice core-based inferences of regional temperature
756 trends in the early Holocene are complicated by uncertain changes in ice sheet surface elevation
757 (e.g., Axford et al., 2021), but increasing $\delta^{18}O_{lw}$ values from Lake N14 provide corroborating
758 direct evidence for continued climate amelioration in this region throughout the first ~1500 years
759 of the Holocene. Chironomid-inferred temperatures at Lake N14 were similar to, but did not
760 exceed, modern summer temperatures by ~10,500 cal yr BP. This record does not extend into the
761 middle Holocene and therefore does not address when maximum Holocene warmth occurred,
762 thus, we cannot further assess the recent finding that peak warmth may have been delayed to the
763 middle Holocene in the south, contrasting with early Holocene peak warmth in other parts of
764 Greenland (Larocca et al., 2020; Axford et al., 2021). This is a potential subject for future work.

765 Conversely, chironomid assemblages suggest that summer temperatures for much of the
766 first millennium of the Holocene were in fact surprisingly cold, after an initial abrupt but short-
767 lived rise to full interglacial summer temperatures at the end of the YD (Fig. 4). In parallel, at the
768 end of the YD, sulfur concentrations in 19-N14-N7 briefly increased before immediately
769 returning to relatively low concentrations in the early Holocene (~11,600 - 10,900 cal yr BP; 297
770 - 269 cm; Fig. 4). Low abundance of marine dinoflagellates from Lake N23 sediments also occur
771 during this time (~11,700 - 10,200 cal yr BP; Ljung and Björck, 2004). Increased sea ice cover
772 driving reductions in sea spray (and, therefore, sulfur concentrations and marine dinoflagellate
773 presence) is consistent with chironomid assemblages in this period that are very low in diversity
774 and dominated by cold stenotherms (Fig. 4). The closest analogs are found only at the highest
775 latitudes in the Arctic today (Medeiros et al., 2022). Dinoflagellate cyst assemblages from
776 HU90-013-013P (~270 km off the southern coast of Greenland) suggest relatively low sea ice
777 cover from 11,500 - 9000 cal yr BP (Fig. 6; Solignac et al., 2004; de Vernal and Hillaire-Marcel,

2006) but again, this record is far from the coast. Sea-surface salinity remained low through much of the early Holocene at this site due to continued freshwater inputs (de Vernal and Hillaire-Marcel, 2006). Further north along Greenland's western coast, dinoflagellate cyst assemblages from marine cores at site SA13-ST3 (64°26.74'N, 52°47.64'W; ~635 km northwest of Lake N14) indicate that summer sea-surface temperatures were relatively cool (0 - 6°C) and sea ice cover was extensive (4 - 10 months per year) from ~12,000 - 10,000 cal yr BP (Allan et al., 2021). ^{10}Be exposure ages from around Narsarsuaq (south Greenland) indicate that the Greenland Ice Sheet retreated to within its late Holocene extent between 11,100 - 10,600 cal yr BP (Carlson et al., 2014), roughly coincident with the evidence for increased sea ice cover from Lake N14. According to moraine chronologies from the Godthåbsfjord and Buksefjord systems of West Greenland, the Greenland Ice Sheet retreated from the outer coast between 11,400 - 10,400 cal yr BP and 10,700 - 10,100 cal yr BP, respectively (Larsen et al., 2014). When combined, this evidence may indicate that meltwater contributions from south Greenland enhanced coastal sea ice formation. Overall, it appears plausible that coastal sea ice could explain the sulfur concentrations and unexpected chironomid assemblage results from Lake N14 in the early Holocene.

6. Conclusions

Diatom assemblages and geochemistry of Lake N14 sediments indicate a transition from marine to lacustrine sediments before the deepest radiocarbon age from this record at 13,605 (13,480-13770; 2σ) cal yr BP (341 cm). This confirms previous findings that the coastal area of southernmost Greenland deglaciated earlier than other areas of Greenland (Björck et al., 2002;

Levy et al., 2020). We find that the $\delta^{18}O$ values of subfossil chironomid head capsules, aquatic moss macrofossils, and aquatic moss cellulose reliably record shifts in lake water $\delta^{18}O$ (and precipitation $\delta^{18}O$ at our site). Changes in temperature, precipitation source/path, and precipitation seasonality together drove changes in precipitation $\delta^{18}O$ at Lake N14 during the YD-Holocene transition and the Preboreal Oscillation that parallel (but were larger in magnitude than) changes over central Greenland. This supports that there was a latitudinal gradient in the magnitude of climate shifts over Greenland during the YD and Preboreal Oscillation, possibly due to varying distance from the zone of North Atlantic Deep Water formation during times of AMOC perturbations (Buizert et al., 2014; 2018).

Region-wide comparisons support the use of a paleothermometer coefficient of ~0.33‰/°C to estimate the temperature changes associated with YD precipitation $\delta^{18}O$ changes at Lake N14. Applying this coefficient, which intrinsically accounts for shifts in atmospheric circulation and seasonality that affected past precipitation $\delta^{18}O$ values, broadly suggests ~18°C ± 7°C of annual warming at the YD-Holocene transition. Chironomid species assemblages indicate YD summers at Lake N14 were ~9°C cooler than modern summers and warmed ~6°C at the YD-Holocene transition. The contrast between summer and annual temperature reconstructions supports the long-standing hypothesis of enhanced seasonality during the YD (Björck et al., 2002; Denton et al., 2005), although chironomid species assemblages suggest colder, harsher summer conditions than previously inferred from algal communities at Lake N14 (Björck et al., 2002). Following the YD, reconstructed $\delta^{18}O_{lw}$ values gradually increased, likely reflecting increasing annual temperatures. Counterintuitively though, after an initial Holocene summer warming and increase in chironomid diversity, cold-indicator chironomid taxa re-established

dominance at Lake N14 from ~11,100 - 10,600 cal yr BP. This may suggest short ice-free seasons or strong suppression of lake water temperatures despite overall regional warming.

Acknowledgments

This work was made possible through financial support from the U.S. National Science Foundation (NSF) Polar Programs award number 2002515. We thank Christine Lee, Annika Hansen, Everett Lasher, and Laura Larocca for assistance with lab work. Additional thanks go to Laura Larocca, G. Everett Lasher, Tim Coston, and Aaron Hartz for assistance during field work and the Woods Hole Oceanographic Institution - National Ocean Sciences Accelerator Mass Spectrometry facility for radiocarbon analysis. We also thank the people and Government of Greenland for allowing us to work on their land. Associate Editor Melanie Leng and two anonymous reviewers provided useful feedback. DEMs provided by the Polar Geospatial Center under NSF-OPP awards 1043681, 1559691, and 1542736.

References

Allan, E., de Vernal, A., Seidenkrantz, M.S., Briner, J.P., Hillaire-Marcel, C., Pearce, C., Meire, L., Røy, H., Mathiasen, A.M., Nielsen, M.T., Plesner, J.L., Perner, K., 2021. Insolation vs. meltwater control of productivity and sea surface conditions off SW Greenland during the Holocene. Boreas 50, 631-651.

Alley, R., 2000. The Younger Dryas cold interval as viewed from central Greenland. Quaternary Science Reviews 19, 213-226.

Alley, R.B., Clark, P.U., 1999. The Deglaciation of the Northern Hemisphere: A Global Perspective. Annual Review of Earth and Planetary Sciences 27, 149-182.

Andresen, C.S., Björck, S., Bennike, O., Bond, G., 2004. Holocene climate changes in southern Greenland: evidence from lake sediments. Journal of Quaternary Science 19, 783-795.

Axford, Y., De Vernal, A., Osterberg, E.C., 2021. Past Warmth and Its Impacts During the Holocene Thermal Maximum in Greenland. Annual Review of Earth and Planetary Sciences 49, 279-307.

Badgeley, J.A., Steig, E.J., Hakim, G.J., Fudge, T.J., 2020. Greenland temperature and precipitation over the last 20 000 years using data assimilation. Climate of the Past 16, 1325-1346.

Bakke, J., Lie, Ø., Heegaard, E., Dokken, T., Haug, G.H., Birks, H.H., Dulski, P., Nilsen, T., 2009. Rapid oceanic and atmospheric changes during the Younger Dryas cold period. Nature Geoscience 2, 202-205.

Bennike, O., Björck, S., 2000. Lake sediment coring in South Greenland in 1999. Geology of Greenland Survey Bulletin 186, 60-64.

Bennike, O., Björck, S., Lambeck, K., 2002. Estimates of South Greenland Lateglacial ice limits from a new relative sea level curve. Earth and Planetary Science Letters 197, 171-186.

Björck, S., Bennike, O., Rosén, P., Andresen, C.S., Bohncke, S., Kaas, E., Conley, D.J., 2002. Anomalously mild Younger Dryas summer conditions in southern Greenland. Geology 30, 427-430.

Björck, S., Rundgren, M., Ingolfsson, O., Funder, S., 1997. The Preboreal oscillation around the Nordic Seas: terrestrial and lacustrine responses. Journal of Quaternary Science 12, 455-465.

Blaauw, M., Christen, J.A., 2011. Flexible paleoclimate age-depth models using an autoregressive gamma process. Bayesian Analysis 6, 457-474.

Bowen, G. J., 2022. The Online Isotopes in Precipitation Calculator, version 3.1. http://www.waterisotopes.org.

Bowen G. J., Wassenaar L. I., Hobson K. A., 2005. Global application of stable hydrogen and oxygen isotopes to wildlife forensics. *Oecologia* **143**, 337-348, doi:10.1007/s00442-004-1813-y.

Boyle, J.F., 2000. Rapid elemental analysis of sediment samples by isotope source XRF. Journal of Paleolimnology 23, 213-221.

Brendel, O., Iannetta, P.P.M., Stewart, D., 2000. A rapid and simple method to isolate pure alpha-cellulose. Phytochemical Analysis 11, 7-10.

Briner, J.P., McKay, N.P., Axford, Y., Bennike, O., Bradley, R.S., de Vernal, A., Fisher, D., Francus, P., Fréchette, B., Gajewski, K., Jennings, A., Kaufman, D.S., Miller, G.,

Rouston, C., Wagner, B., 2016. Holocene climate change in Arctic Canada and Greenland. Quaternary Science Reviews 147, 340-364.

Broecker, W., Andree, M., Wolfli, W., Oeschger, H., Bonani, G., Kennett, J., Peteet, D., 1988. The Chronology of the Last Deglaciation: Implications to the Cause of the Younger Dryas Event. Paleoceanography 3, 1-19.

Buizert, C., Gkinis, V., Severinghaus, J.P., He, F., Lecavalier, B.S., Kindler, P., Leuenberger, M., Carlson, A.E., Vinther, B., Masson-Delmotte, V., White, J.W., Liu, Z., Otto-Bliesner, B., Brook, E.J., 2014. Greenland temperature response to climate forcing during the last deglaciation. Science 345, 1177-1180.

Buizert, C., Keisling, B.A., Box, J.E., He, F., Carlson, A.E., Sinclair, G., DeConto, R.M., 2018. Greenland-Wide Seasonal Temperatures During the Last Deglaciation. Geophysical Research Letters 45, 1905-1914.

Butler, M.G., 1982. A 7-year life cycle for two *Chironomus* species in arctic Alaskan tundra ponds (Diptera: Chironomidae). Can. J. Zool. 60, 58-70.

Butler, M.G., Braegelman, S.D., 2018. Pre-emergence growth and development in the arctic midge *Trichotanypus alaskensis* Brundin. Journal of Limnology 77, 113-120.

Caesar, L., McCarthy, G.D., Thornalley, D.J.R., Cahill, N., Rahmstorf, S., 2021. Current Atlantic Meridional Overturning Circulation weakest in last millennium. Nature Geoscience 14, 118-120.

Cappelen, J., 2019. Climatological Standard Normals 1981-2010 - Denmark, The Faroe Islands and Greenland - Based on Data Published in DMI Reports 18-02, 18-04 and 18-05. DMI Report 18-19, Copenhagen.

Carlson, A.E., Clark, P.U., Haley, B.A., Klinkhammer, G.P., Simmons, K., Brook, E.J., Meissner, K.J., 2007. Geochemical proxies of North American freshwater routing during the Younger Dryas cold event. Proc Natl Acad Sci U S A 104, 6556-6561.

Carlson, A.E., Winsor, K., Ullman, D.J., Brook, E.J., Rood, D.H., Axford, Y., LeGrande, A.N., Anslow, F.S., Sinclair, G., 2014. Earliest Holocene south Greenland ice sheet retreat within its late Holocene extent. Geophysical Research Letters 41, 5514-5521.

Clarke, C.L., Gröcke, D.R., Elias, S., Langdon, P.G., van Hardenbroek, M., 2019. Effects of chemical pretreatment and intra- and inter-specimen variability on δ18O of aquatic insect remains. Journal of Paleolimnology 62, 195-204.

Corcoran, M.C., Thomas, E.K., Morrill, C., 2021. Using a Paired Chironomid $\delta^{18}O$ and Aquatic Leaf Wax $\delta^{2}H$ Approach to Reconstruct Seasonality on Western Greenland During the Holocene. Paleoceanography and Paleoclimatology 36, 1-18.

Dansgaard, W., 1964. Stable isotopes in precipitation. Tellus 16, 436-468.

Dansgaard, W., Clausen, H.B., Gundestrup, N., Hammer, C.U., Johnsen, S.F., Kristinsdottir, P.M., Reeh, N., 1982. A new Greenland deep ice core. Science 218, 1273-1277.

Dansgaard, W., White, J.W., Johnsen, S., 1989. The abrupt termination of the Younger Dryas climate event Nature 339, 532-534.

Denton, G., Alley, R., Comer, G., Broecker, W., 2005. The role of seasonality in abrupt climate change. Quaternary Science Reviews 24, 1159-1182.

de Vernal, A., Hillaire-Marcel, C., 2006. Provincialism in trends and high frequency changes in the northwest North Atlantic during the Holocene. Global and Planetary Change 54, 263-290.

Fawcett, P.J., Ágústsdóttir, A.M., Alley, R.B., Shuman, C.A., 1997. The Younger Dryas Termination and North Atlantic Deep Water Formation: Insights from climate model simulations and Greenland Ice Cores. Paleoceanography 12, 23-38.

Fiłoc, M., Kupryjanowicz, M., Rzodkiewicz, M., Suchora, M., 2018. Response of terrestrial and lake environments in NE Poland to Preboreal cold oscillations (PBO). Quaternary International 475, 101-117.

Firestone, R.B., West, A., Kennett, J.P., Becker, L., Bunch, T.E., Revay, Z.S., Schultz, P.H., Belgya, T., Kennett, D.J., Erlandson, J.M., Dickenson, O.J., Goodyear, A.C., Harris, R.S., Howard, G.A., Kloosterman, J.B., Lechler, P., Mayewski, P.A., Montgomery, J., Poreda, R., Darrah, T., Que Hee, S.S., Smith, A.R., Stich, A., Topping, W., Wittke, J.H., Wolbach, W.S., 2007. Evidence for an extraterrestrial impact 12,900 years ago that contributed to the megafaunal extinctions and the Younger Dryas cooling. Proc Natl Acad Sci U S A 104, 16016 –16021.

Foged, N., 1972. The diatoms in four postglacial deposits in Greenland. Meddelelser om Grønland 194: 1–66.

Foged, N., 1973. Diatoms from Southwest Greenland. Meddelelser om Grønland 194: 1–84.

Foged N., 1977. The diatoms in four postglacial deposits at Godthåbsfjord, West Greenland. Meddelelser om Grønland 199: 1–64.

Francus, P., Lamb, H., Nakagawa, T., Marshall, M., Brown, E., 2009. The potential of high-resolution X-ray fluorescence core scanning: Applications in paleolimnology. PAGES news 17, 93-96.

Gajewski, K., Bouchard, G., Wilson, S. E., Kurek, J., Cwynar, L. C., 2005. Distribution of Chironomidae (Insecta: Diptera) head capsules in recent sediments of Canadian Arctic lakes. Hydrobiologia, 549(1), 131-143.

Grootes, P.M., Stuiver, M., 1997. Oxygen 18/16 variability in Greenland snow and ice with 10−3- to 105-year time resolution. Journal of Geophysical Research: Oceans 102, 26455-26470.

Hendey, N.I., 1964. An Introductory Account of the Smaller Algae of British Coastal Waters. Part V: Bacillariophyceae (Diatoms), Fisheries Investigation Series I. HMSO: London.

Hustedt, F., 1957. Diatomeenflora de Fluss-Systems der Weser im Gebeit der Hansestadt Bremen. Abhandlungen des Naturwissenschaftlichen Vereins zu Bremen 34, 181–440.

IAEA/WMO, 2015. Global Network of Isotopes in Precipitation. The GNIP Database. Accessible at: https://nucleus.iaea.org/wiser.

Jackson, L.C., Biastoch, A., Buckley, M.W., Desbruyères, D.G., Frajka-Williams, E., Moat, B., Robson, J., 2022. The evolution of the North Atlantic Meridional Overturning Circulation since 1980. Nature Reviews Earth & Environment.

Kapsner, W.R., Alley, R., Shuman, C.A., Anandakrishnan, S., Grootes, P.M., 1995. Dominant influence of atmospheric circulation on snow accumulation in Greenland over the past 18,000 years. Nature 373, 52-54.

Keigwin, L.D., Klotsko, S., Zhao, N., Reilly, B., Giosan, L., Driscoll, N.W., 2018. Deglacial floods in the Beaufort Sea preceded Younger Dryas cooling. Nature Geoscience 11, 599-604.

Larocca, L.J., Axford, Y., Bjørk, A.A., Lasher, G.E., Brooks, J.P., 2020. Local glaciers record delayed peak Holocene warmth in south Greenland. Quaternary Science Reviews 241, 106421.

Larsen, N.K., Funder, S., Kjær, K.H., Kjeldsen, K.K., Knudsen, M.F., Linge, H., 2014. Rapid early Holocene ice retreat in West Greenland. Quaternary Science Reviews 92, 310-323.

Lasher, G.E., Axford, Y., 2019. Medieval warmth confirmed at the Norse Eastern Settlement in Greenland. Geology 47, 267-270.

Lasher, G.E., Axford, Y., McFarlin, J.M., Kelly, M.A., Osterberg, E.C., Berkelhammer, M.B., 2017. Holocene temperatures and isotopes of precipitation in Northwest Greenland recorded in lacustrine organic materials. Quaternary Science Reviews 170, 45-55.

Law, A.C., Anderson, N.J., McGowan, S., 2015. Spatial and temporal variability of lake ontogeny in south-western Greenland. Quaternary Science Reviews 126, 1-16.

Levy, L.B., Larsen, N.K., Knudsen, M.F., Egholm, D.L., Bjørk, A.A., Kjeldsen, K.K., Kelly, M.A., Howley, J.A., Olsen, J., Tikhomirov, D., Zimmerman, S.R.H., Kjær, K.H., 2020. Multi-phased deglaciation of south and southeast Greenland controlled by climate and topographic setting. Quaternary Science Reviews 242.

Leydet, D.J., Carlson, A.E., Teller, J.T., Breckenridge, A., Barth, A.M., Ullman, D.J., Sinclair, G., Milne, G.A., Cuzzone, J.K., Caffee, M.W., 2018. Opening of glacial Lake Agassiz's eastern outlets by the start of the Younger Dryas cold period. Geology 46, 155-158.

Ljung, K., Björck, S., 2004. A lacustrine record of the Pleistocene-Holocene boundary in southernmost Greenland. Gff 126, 273-278.

Lombino, A., Atkinson, T., Brooks, S.J., Gröcke, D.R., Holmes, J., Jones, V.J., Marshall, J.D., 2021. Experimental determination of the temperature dependence of oxygen-isotope fractionation between water and chitinous head capsules of chironomid larvae. Journal of Paleolimnology 66, 117-124.

Long, A.J., Woodroffe, S.A., Roberts, D.H., Dawson, S., 2011. Isolation basins, sea-level changes and the Holocene history of the Greenland Ice Sheet. Quaternary Science Reviews 30, 3748-3768.

Mayewski, P.A., Meeker, L.D., Whitlow, S., Twickler, M.S., Morrison, M.C., Alley, R.B., Bloomfield, P., Taylor, K., 1993. The atmosphere during the Younger Dryas. Science 261, 195-197.

McManus, J.F., Francois, R., Gherardi, J.M., Keigwin, L.D., Brown-Leger, S., 2004. Collapse and rapid resumption of Atlantic meridional circulation linked to deglacial climate changes. Nature 428, 834-837.

Medeiros, A.S., Chipman, M., Francis, D.R., Hamerlik, L., Langdon, P., Puleo, P.J.K., Schellinger, G., Steigleder, R., Walker, I.R., Woodroffe, S., and Axford, Y. 2022. A continent-scale chironomid training set for reconstructing arctic temperatures. Quaternary Science Reviews 294, 107728.

Nusbaumer, J., Alexander, P.M., LeGrande, A.N., Tedesco, M., 2019. Spatial Shift of Greenland Moisture Sources Related to Enhanced Arctic Warming. Geophysical Research Letters 46, 14,723–714,731.

Oliver, D.R., 1968. Adaptations of Arctic Chironomidae. Annales Zoologici Fennici 5, 111-118.

Palmer, A.J.M., Abbott, W.H., 1986. Diatoms as indicators of sea-level change. In Sea-Level Research, Van De Plassche O (ed.) Geo Books: Norwich, UK; 457–487.

Patrick, R., Reimer, C.W., 1966. The diatoms of the United States exclusive of Hawaii and Alaska, Vol. 1. Monograph of the Academy of Natural Sciences of Philadelphia 13.

Patrick, R., Reimer, C.W., 1975. The diatoms of the United States exclusive of Hawaii and Alaska, Vol. 2, Part 1. Monograph of the Academy of Natural Sciences of Philadelphia 13.

Porter, C., Morin, P., Howat, I., Noh, M.J., Bates, B., Peterman, K., Keesey, S., Schlenk, M., Gardiner, J., Tomko, K., Willis, M., Kelleher, C., Cloutier, M., Husby, E., Foga, S., Nakamura, H., Platson, M., Wethington, M., Williamson, C., Bauer, G., Enos, J., Arnold, G., Kramer, W., Becker, P., Doshi, A., D'Souza, C., Cummens, P., Laurier, F., Bojesen, M., 2018, "ArcticDEM", https://doi.org/10.7910/DVN/OHHUKH, Harvard Dataverse, V1, Accessed 6/13/2022.

Porter, T.J., Schoenemann, S.W., Davies, L.J., Steig, E.J., Bandara, S., Froese, D.G., 2019. Recent summer warming in northwestern Canada exceeds the Holocene thermal maximum. Nat Commun 10, 1631.

Rahmstorf, S., Box, J.E., Feulner, G., Mann, M.E., Robinson, A., Rutherford, S., Schaffernicht, E.J., 2015. Exceptional twentieth-century slowdown in Atlantic Ocean overturning circulation. Nature Climate Change 5, 475-480.

Rasmussen, S.O., Andersen, K.K., Svensson, A.M., Steffensen, J.P., Vinther, B.M., Clausen, H.B., Siggaard-Andersen, M.L., Johnsen, S.J., Larsen, L.B., Dahl-Jensen, D., Bigler, M., Röthlisberger, R., Fischer, H., Goto-Azuma, K., Hansson, M.E., Ruth, U., 2006. A new Greenland ice core chronology for the last glacial termination. Journal of Geophysical Research 111, 1-16.

Rasmussen, S.O., Vinther, B.M., Clausen, H.B., Andersen, K.K., 2007. Early Holocene climate oscillations recorded in three Greenland ice cores. Quaternary Science Reviews 26, 1907-1914.

Reimer, P.J., Austin, W.E.N., Bard, E., Bayliss, A., Blackwell, P.G., Bronk Ramsey, C., Butzin, M., Cheng, H., Edwards, R.L., Friedrich, M., Grootes, P.M., Guilderson, T.P., Hajdas, I., Heaton, T.J., Hogg, A.G., Hughen, K.A., Kromer, B., Manning, S.W., Muscheler, R., Palmer, J.G., Pearson, C., van der Plicht, J., Reimer, R.W., Richards, D.A., Scott, E.M., Southon, J.R., Turney, C.S.M., Wacker, L., Adolphi, F., Büntgen, U., Capano, M., Fahrni, S.M., Fogtmann-Schulz, A., Friedrich, R., Köhler, P., Kudsk, S., Miyake, F., Olsen, J., Reinig, F., Sakamoto, M., Sookdeo, A., Talamo, S., 2020. The IntCal20 Northern Hemisphere Radiocarbon Age Calibration Curve (0–55 cal kBP). Radiocarbon 62, 725-757.

Renssen, H., Mairesse, A., Goosse, H., Mathiot, P., Heiri, O., Roche, D.M., Nisancioglu, K.H., Valdes, P.J., 2015. Multiple causes of the Younger Dryas cold period. Nature Geoscience 8, 946-949.

Riis, T., Olesen, B., Katborg, C.K., Christoffersen, K.S., 2010. Growth Rate of an Aquatic Bryophyte (*Warnstorfia fluitans* (Hedw.) Loeske) from a High Arctic Lake: Effect of Nutrient Concentration. Arctic 63, 100-106.

Rohling, E.J., Yu, J., Heslop, D., Foster, G.L., Opdyke, B., Roberts, A.P., 2021. Sea level and deep-sea temperature reconstructions suggest quasi-stable states and critical transitions over the past 40 million years. Sci Adv 7, 1-17.

Severinghaus, J.P., Sowers, T., Brook, E.J., Alley, R.B., Bender, M.L., 1998. Timing of abrupt climate change at the end of the Younger Dryas interval from thermally fractionated gases in polar ice. Nature 391, 141-146.

Shakun, J.D., Carlson, A.E., 2010. A global perspective on Last Glacial Maximum to Holocene climate change. Quaternary Science Reviews 29, 1801-1816.

Sime, L.C., Hopcroft, P.O., Rhodes, R.H., 2019. Impact of abrupt sea ice loss on Greenland water isotopes during the last glacial period. Proc Natl Acad Sci U S A 116, 4099-4104.

Solignac, S., de Vernal, A., Hillaire-Marcel, C., 2004. Holocene sea-surface conditions in the North Atlantic—contrasted trends and regimes in the western and eastern sectors (Labrador Sea vs. Iceland Basin). Quaternary Science Reviews 23, 319-334.

Spaulding, S.A., Potapova, M.G., Bishop, I.W., Lee, S.S., Gasperak, T.S., Jovanoska, E., Furey, P.C., Edlund, M.B., 2021. Diatoms.org: supporting taxonomists, connecting communities. Diatom Research 36, 291-304.

Steenfelt, A., Kolb, J., Thrane, K., 2016. Metallogeny of South Greenland: A review of geological evolution, mineral occurrences and geochemical exploration data. Ore Geology Reviews 77, 194-245.

Stenni, B., Masson-Delmotte, V., Selmo, E., Oerter, H., Meyer, H., Röthlisberger, R., Jouzel, J., Cattani, O., Falourd, S., Fischer, H., Hoffmann, G., Iacumin, P., Johnsen, S.J., Minster, B., Udisti, R., 2010. The deuterium excess records of EPICA Dome C and Dronning Maud Land ice cores (East Antarctica). Quaternary Science Reviews 29, 146-159.

Sternberg, L., Ellsworth, P.F., 2011. Divergent biochemical fractionation, not convergent temperature, explains cellulose oxygen isotope enrichment across latitudes. PLoS One 6, e28040.

Stuiver, M., Reimer, P.J., and Reimer, R.W., 2022, CALIB 8.2 [WWW program] at http://calib.org, accessed 2022-4-13.

Tokeshi, M., 1995. Life cycles and population dynamics, in: Armitage, P.D., Cranston, P.S., Pinder, L.C.V. (Eds.), The Chironomidae: the biology and ecology of non-biting midges. Springer, Dordrecht, pp. 225-268.

van Hardenbroek, M., Chakraborty, A., Davies, K.L., Harding, P., Heiri, O., Henderson, A.C.G., Holmes, J.A., Lasher, G.E., Leng, M.J., Panizzo, V.N., Roberts, L., Schilder, J., Trueman, C.N., Wooller, M.J., 2018. The stable isotope composition of organic and inorganic fossils in lake sediment records: Current understanding, challenges, and future directions. Quaternary Science Reviews 196, 154-176.

van der Werff, H., Huls, H., 1958–1974. Diatomeenflora van Nederland. Koeltz Scientific Books: Koenigstein.

Verbruggen, F., Heiri, O., Reichart, G.J., De Leeuw, J.W., Nierop, K.G.J., Lotter, A.F., 2010. Effects of chemical pretreatments on δ18O measurements, chemical composition, and morphology of chironomid head capsules. Journal of Paleolimnology 43, 857-872.

Wooller, M.J., Francis, D., Fogel, M.L., Miller, G.H., Walker, I.R., Wolfe, A.P., 2004. Quantitative paleotemperature estimates from $\delta^{18}O$ of chironomid head capsules preserved in arctic lake sediments. Journal of Paleolimnology 31, 267-274.

Zhu, J., Lücke, A., Wissel, H., Mayr, C., Ohlendorf, C., Zolitschka, B., 2014. Characterizing oxygen isotope variability and host water relation of modern and subfossil aquatic mosses. Geochimica et Cosmochimica Acta 130, 212-228.